2019

Seasonal Variability of the Co2-System Throughout the Chesapeake Bay Mainstem

Jaclyn Rain Friedman
William & Mary - Virginia Institute of Marine Science, jackie.friedman17@gmail.com

Seasonal Variability of the CO_2-System Throughout the Chesapeake Bay Mainstem

A Thesis

Presented to

The Faculty of the School of Marine Science

The College of William and Mary in Virginia

In Partial Fulfillment

of the Requirements for the Degree of

Master of Science

by

Jaclyn R. Friedman

August 2019

APPROVAL PAGE

This thesis is submitted in partial fulfillment of

the requirements for the degree of

Master of Science

Jaclyn R. Friedman

Approved by the Committee, August 2019

Elizabeth H. Shadwick, Ph.D.
Committee Chair / Advisor

Juliette L. Smith, Ph.D.
Committee Chair / Advisor

Marjorie A. M. Friedrichs, Ph.D.

William G. Reay, Ph.D.

TABLE OF CONTENTS

ACKNOWLEDGEMENTS v

LIST OF TABLES vi

LIST OF FIGURES vii

ABSTRACT viii

1. INTRODUCTION 2

1.1 Motivation 2

1.2 Thesis Objectives 5

2. SCIENTIFIC BACKGROUND 6

2.1 Dissolved Inorganic Carbon (DIC) 6

2.2 Total Alkalinity (TA) 7

2.3 pH 8

2.4 Partial Pressure of CO_2 (pCO_2) 8

2.5 Saturation State of Calcium Carbonate (Ω) 8

3. METHODS 9

3.1 Field Methods 9

3.2 Laboratory Methods 11

3.3 Assignment of Geographic Regions 13

3.4 Estimation of Total Alkalinity During the Winter Season 15

3.5 Air-sea CO_2 Flux 15

3.6 Mass Balance of DIC 17

3.7 Uncertainty Analysis 19

4. RESULTS 20

4.1 Representativeness of Mainstem Cruises 20

4.2 Seasonality of CO_2 system Parameters Throughout the Mainstem 20

4.3 Temperature-normalized pCO_2 and Air-sea CO_2 Fluxes 23

4.4 Seasonal Mass Balance of DIC 25

4.5 Net Community Production 26

5. DISCUSSION 28

5.1 Net Community Production in the Context of Earlier Estimates 28

5.2 Comparison with Other Estuarine and Coastal Ocean Systems 29

6. SUMMARY and CONCLUSIONS 33

LITERATURE CITED 55

Acknowledgements

The completion of this thesis would not be possible without the help of numerous people who have supported not only the research conducted in pursuit of my master's degree, but my personal and professional goals as well. I would like to thank both of my advisors, Dr. Elizabeth H. Shadwick and Dr. Juliette L. Smith, for the opportunity to conduct new and exciting research in a variety of environments. The skills I have gained while working with both the inorganic carbon chemistry lab and HAB lab are immeasurable. I would also like to thank my committee members, Dr. Marjy Friedrichs and Dr. William Reay, for providing insight on the Chesapeake Bay system, as well as providing guidance, direction, and support throughout my thesis. Thank you to Olivia De Meo for dedicating much time to this project, including sample collection and analysis and data processing, and for your friendship through it all.

In addition, I would like to thank the Chesapeake Bay Program's Water Quality Monitoring Program. In particular, Dr. John Donat and Mark Trice, as well as Virginia's Department of Environmental Quality and the captain, crew, and scientists onboard Old Dominion University's vessel, the R/V Fay Slover, as well as Maryland's Department of Natural Resources and the captain, crew, and scientists onboard their vessel, the R/V Kerhin. Thanks to Fei Da for the MATLAB guidance and insightful scientific conversations from which I have learned so much. I would also like to thank Pierre St-Laurent, who has provided excellent feedback for my many questions. This project would not be complete without Dr. Raymond Najjar and Dr. Maria Herrmann; I appreciate your scientific input on all things CO_2-system and Chesapeake Bay. Without these collaborations, the research presented in this thesis would not be possible.

Thanks to the individuals and departments that keep VIMS operating (e.g., Vessels, ITNS, Facilities). I would like to specially thank Mark Brabham and Mark Rogers for their encouragement while pursuing many sustainable initiatives during my time at VIMS. I would like to thank the Office of Academic Studies for supporting graduate students and life at VIMS, and for hosting my favorite event, writing boot camp. Thank you to Marta Sanderson, Sarah Pease, Michelle Onofrio, and Gao Han for teaching me new skills and for the opportunity to learn with you. To Dr. Rose Martin, for encouraging me to investigate what I am interested in and for the support through it all. Finally, I would like to thank my friends, family, and the VIMS community for everything. Friends, your humor and advice make everything in life much easier. I would especially like to thank Mar for being the best lab and office mate that anyone could ask for. I will forever be grateful to have had your companionship through our time at VIMS and all that is to come. I am forever thankful to have a family that supports each of my goals and for encouraging me to pursue all my passions throughout each stage of life; I would not be who I am today without you. Finally, a huge thanks to Matt for keeping me afloat all these years. Without you and your unending patience, this would have been a much more difficult journey.

LIST OF TABLES

1. Dates of seasonal CO_2 system sample collection 36
2. Geographic location of each station 37
3. Seasonal mean values of CO_2 system parameters in the surface mixed layer of each region 38
4. Seasonal mean values of CO_2 system parameters in the subsurface waters of each region 39
5. Wind speed and surface used to calculate air-sea flux in each region 40
6. Partitioning of physical and biological drivers of DIC variability 41
7. Net Community Production throughout the CB mainstem 42

LIST OF FIGURES

1. Changes to atmospheric and surface water CO_2 and pH in the central Pacific Ocean 43

2. Equilibrium distribution of carbonate species....44

3. Regional partitioning of CBMP monitoring stations in the Chesapeake Bay mainstem 45

4. Seasonal surface salinity at each station 46

5. Linear regression analysis of TA and DIC with salinity 47

6. Monthly observations of CBMP surface temperature and salinity 48

7. Seasonality in TA at the mouth of the Susquehanna River 49

8. Average seasonal cycle of CBMP and CO_2 system parameters in the surface mixed layer 50

9. Average seasonal cycle of CBMP and CO_2 system parameters in subsurface waters 51

10. Spatial and temporal variability of air-sea CO_2 flux 52

11. Mass balance partitioning of DIC in the surface mixed layer....53

12. Mass balance partitioning of DIC throughout the entire water column 54

ABSTRACT

Declining water quality, in addition to hypoxia and eutrophication, may have a significant impact on the seasonality of biogeochemical parameters throughout the mainstem of the Chesapeake Bay. The carbonate (CO_2) system in the Chesapeake Bay experiences seasonal and spatial complexities and is influenced by both natural and anthropogenic variability. Although site-specific studies investigating CO_2-system variability exist within the Chesapeake Bay, few studies have investigated the seasonality of the CO_2-system throughout the entire mainstem. Additionally, recent comprehensive studies investigating over 50 estuaries along the East Coast of the United States suggest that estuarine systems are heterotrophic and act as sources of CO_2 to the atmosphere; this current paradigm does not apply to the mainstem of the Chesapeake Bay. The research presented here will assess the net annual source/sink status of atmospheric CO_2 in the mainstem, along with an evaluation of annual net community production and trophic status, which is assessed based on a mass balance of dissolved inorganic carbon (DIC).

Discrete observations of DIC and total alkalinity (TA) are collected at 17 stations throughout the mainstem of the Bay on four cruises between November 2016 and July 2017. The latitudinal salinity gradient along the mainstem of the Bay results in elevated DIC and TA concentrations at the mouth of the Bay associated with inflowing Atlantic Ocean waters. Minimum concentrations of DIC and TA are associated with fresher waters, delivered mainly by the Susquehanna River, at the head of the Bay. The spatial gradients in DIC and TA are observed regardless of season. Spatial variability of the partial pressure of CO_2 (pCO_2) is observed throughout the surface waters of the estuary, with undersaturation of CO_2 with respect to the atmosphere in the upper Bay over the complete seasonal cycle, and supersaturation with respect to atmospheric CO_2 in the lower Bay during the warm seasons. The spatial and seasonal distribution of pH and saturation state of aragonite (Ω) are more variable throughout the mainstem, as the seasonality of these parameters are different in each region. The physical (air-sea CO_2 exchange and mixing) and biological (photosynthesis and respiration) drivers of CO_2-system seasonality is examined throughout the mainstem Bay. In the deep, northern channel of the mainstem, seasonal CO_2-system variability is larger than the lower Bay regions that are more directly influenced by exchange with Atlantic Ocean shelf waters. Overall, when averaged over the 2016/2017 seasonal cycle used in this analysis, the mainstem of the Chesapeake Bay is found to be net heterotrophic and a sink of atmospheric CO_2.

Seasonal Variability of the CO_2-system Throughout the Chesapeake Bay Mainstem

1. Introduction

1.1 Motivation

In the open ocean, the uptake of anthropogenic carbon dioxide (CO_2) has decreased the surface ocean pH by 0.1 standard units over the past century (Figure 1; Dore et al., 2009; Orr et al., 2005). In estuarine systems, the interactions between the atmosphere, the land, the coastal ocean, and the sediments are closely linked in space and time, but the impact of rising atmospheric CO_2 on the CO_2-system is less well understood. Coastal systems are influenced by additional anthropogenic stressors, such as urban development and atmospheric deposition of nitrogen from fossil fuel combustion, that may have compensatory or additive effects on changes to the CO_2-system (Da et al., 2018; Doney, 2010; Sunda & Cai, 2012). Estuaries represent dynamic systems that connect terrestrial and aquatic environments through mixing of riverine and oceanic waters. Nearshore systems may experience greater seasonal and interannual variability than their open ocean counterparts due to their sensitivity to changes in highly variable riverine discharge.

The Chesapeake Bay (CB) is the largest estuary in the United States, thus making it an important part of the regional history and economy. The CB watershed encompasses an area of 164,200 km^2 over 6 states (Delaware, Maryland, New York, Pennsylvania, Virginia, and West Virginia) and the District of Columbia. The population throughout the watershed has grown exponentially, with a 117% increase between 1950 and 2017 (Chesapeake Bay Program, 2018). Within the watershed, there are many major cities and industrial areas (e.g., Baltimore, Washington D.C., Hampton-Roads), as well as agricultural zones (e.g., Eastern Shore of VA and Lancaster, PA). Of the CB watershed, 57% of land is comprised of forests, 30% of land use is agricultural, and the remaining

13% contains regions of human development (United States Department of Agriculture, 2018; Chesapeake Bay Program, 2018). Changes in land use and the introduction of more developed and populated areas coincide with greater transport of nutrients to the CB, as urban landscapes have a much higher nutrient export than agricultural and forested landscapes (Castro et al., 2003; Najjar et al., 2010). During the spring season, when the delivery of freshwater to the CB mainstem is the greatest, delivery of nitrogen is also highest (Kemp et al., 1992; Najjar et al., 2010). The Susquehanna River delivers approximately 48% of freshwater discharge to the CB mainstem, with the Potomac River contributing 16%, and the James, Rappahannock, and York Rivers combined contributing 19%. The remaining 17% of freshwater delivery is from smaller tributaries on the western shore of the CB and rivers and streams along the eastern shore of Maryland and Virginia (Xu et al., 2012).

Hypoxia in the deep CB mainstem is stimulated by eutrophication and the resulting production of excess organic matter (Hagy et al., 2004; Harding et al., 2014, 2016; Zimmerman & Canuel, 2000). If the organic matter generated by phytoplankton growth is not consumed locally in surface waters or laterally exported from the region, it sinks and subsequent remineralization leads to elevated concentrations of dissolved inorganic carbon (DIC) at depth (e.g., Cai et al., 2011; Cai et al., 2004; Gobler & Baumann, 2016), which is an ongoing issue. When the CB mainstem is stratified, reduced vertical exchange of surface and bottom water inhibits the replenishment of DO from the atmosphere, leading to the development of large volumes of hypoxic water (Kemp et al., 1992; Irby et al., 2016). Reduced vertical exchange also prevents the ventilation of high DIC waters at depth with lower DIC surface waters and equilibration with the atmosphere. This annual occurrence

of low DO and high DIC concentrations in subsurface waters has been well documented in a site-specific summer study in the upper CB mainstem by Cai et al. (2017). This pattern of low DO and high DIC concentrations in subsurface waters has also been reported in many other coastal and estuarine ecosystems, including the Baltic Sea (Schneider, 2011) and the Gulf of Mexico (Hu et al., 2017; Schneider, 2011).

While estuaries encompass only 4% of total coastal ocean surface area, they are generally thought to be heterotrophic systems that act as net sources of CO_2 to the atmosphere, playing a disproportionality large role in the coastal carbon cycle relative to their size (Borges, 2005; Joesoef et al., 2015; Hermann et al., 2015; Laruelle et al., 2015; Laruelle et al., 2010). More specifically, estuaries along the East Coast of the United States outgas approximately 110 g C m^{-2} yr^{-1} (Najjar et al., 2018).

To investigate if the CB fits this estuarine paradigm, a novel partitioning of the CO_2-system over a seasonal scale is conducted to determine the trophic status of the CB mainstem via a quantification of annual net community production (NCP). In this study the seasonal magnitude and variability of CO_2-system parameters throughout the CB mainstem, providing an important next step in understanding carbon budgets for other estuarine systems as well as the coastal ocean. A recent model-based study provides greater temporal and spatial resolution than previous work investigating the source or sink status of atmospheric CO_2 throughout the CB mainstem (Shen et al., 2019). While valuable, the model was not compared to discrete observations from the winter season (Shen et al., 2019). In order to accurately assess the source/sink status of atmospheric CO_2 in the CB mainstem on the annual scale, CO_2-system observations from each season are necessary. Thus, the current study uses discrete observations from four seasons from autumn 2016 to

summer 2017 to investigate the air-sea CO_2 flux from CB surface waters on both seasonal and annual scales. Although the trophic status of the CB mainstem has been evaluated previously on the basis of organic carbon and nitrogen (Feng et al., 2015; Kemp et al., 1997), this analysis, based on a mass balance of DIC, contributes new insights to the seasonality of the CB CO_2-system.Discrete shipboard measurements are used to partition the seasonality of the CO_2-system into physical and biological drivers, yielding an assessment of seasonal NCP, trophic status, and air-sea CO_2 exchange for four regions within the CB mainstem, and the mainstem as a whole.

1.2 Thesis Objectives

This research will determine the seasonal variability of the CO_2-system throughout the entire CB mainstem and provide novel insight into the role that estuaries play in the coastal carbon cycle. Previous, site-specific CO_2-system studies have been conducted throughout the CB (Cai et al., 2017; Shadwick et al., 2019), but information regarding the seasonality of CO_2-system parameters throughout the entire mainstem is lacking, despite recent work (e.g., Shen et al., 2019; Brodeur et al., 2019). This thesis has three overarching objectives: 1) to investigate the seasonal variability of the CO_2-system throughout the entire CB mainstem through the partitioning of physical and biological drivers, 2) to quantify estimates of both seasonal and annual NCP to determine trophic status of the mainstem, and 3) to determine the seasonal and annual source/sink status of the surface waters with respect to atmospheric CO_2. These objectives were achieved using a combination of seasonal shipboard observations of the CO_2-system and a DIC mass-balance approach; details are given in Section 3.

2. Scientific Background – The CO_2-system in Seawater

The reaction between CO_2 and seawater is described by the equilibrium reactions given below. CO_2 reacts with seawater to form carbonic acid (H_2CO_3, Eq. 1.1); this weak acid rapidly dissociates to form bicarbonate (HCO_3^-, Eq. 1.2) and carbonate (CO_3^{2-}, Eq. 1.3) ions:

$$CO_{2(aq)} + H_2O \leftrightarrow H_2CO_3 \quad \text{Eq. 1.1}$$

$$H_2CO_3 \leftrightarrow H^+ + HCO_3^- \quad \text{Eq. 1.2}$$

$$HCO_3^- \leftrightarrow H^+ + CO_3^{2-} \quad \text{Eq. 1.3}$$

The abundance of each species in seawater at its current pH (~8.1) is shown in Figure 2 with HCO_3^- being the dominant species, followed by CO_3^{2-} and dissolved CO_2.

This research will focus on DIC, total alkalinity (TA), pH, the partial pressure of CO_2 (pCO_2), and the saturation state of calcium carbonate (Ω). Four carbonate system parameters (DIC, TA, pH, and pCO_2) can be determined analytically. Any two of these four can be used to compute the full suite of carbonate system parameters using the equilibration constants for the system of equations that fully describe the dissolution of CO_2 in seawater (e.g., Zeebe & Wolf-Galdrow, 2001).

2.1 Dissolved Inorganic Carbon (DIC)

DIC is defined as the sum of all dissolved inorganic carbon species (Zeebe & Wolf-Gladrow, 2001; Eq. 2)

$$DIC = [H_2CO_3] + [CO_2] + [HCO_3^-] + [CO_3^{2-}] \quad \text{Eq. 2}$$

2.2 Total Alkalinity (TA)

TA can simply be defined as the charge imbalance of major conservative ions in seawater (Eq. 3). The sum of charges of the major cations of strong bases (e.g., Na^+, K^+, Mg^{2+}, Ca^{2+}) are not completely balanced by the sum of the major anions of strong acids (e.g., Cl^-, SO_4^{2-}), leading to the charge difference that is alkalinity (Zeebe & Wolf-Galdrow, 2001)

$$TA = \Sigma(\text{cations}) - \Sigma(\text{anions}) \qquad \text{Eq. 3}$$

By neglecting the minor acids and bases in seawater, TA is approximated by:

$$TA = [HCO_3^-] + 2[CO_3^{2-}] + [B(OH)_4^-] + [OH^-] - [H^+] \qquad \text{Eq. 4}$$

Total Alkalinity is a conservative quantity such that its concentration is not affected by changes in temperature or pressure. TA is influenced by a number of processes including: the dissolution or precipitation of calcium carbonate ($CaCO_3$) and the biological uptake of nitrate (Zeebe & Wolf-Galdrow, 2001). The dissolution of 1 mole of $CaCO_3$ increases the concentration of TA by 2 moles, conversely the precipitation of 1 mole of $CaCO_3$ decreases TA by 2 moles. An increase in TA associated with photosynthesis occurs during the uptake of nitrate (NO_3^-) by phytoplankton and algae. The uptake of one mole of NO_3^- results in a one mole increase in alkalinity. This assimilation of nitrate by plants is assumed to be parallel to the release of OH^-, thus further increasing the concentrations of TA. The uptake of ammonium (NH_4^+), however, is balanced by the release of H^+, thereby decreasing TA (Brewer & Goldman, 1976; Zeebe & Wolf-Galdrow, 2001).

2.3 pH

pH is commonly defined as the -log[H^+]. The concentration of H^+ ions is related to the activity of the species using an activity coefficient, γH^+. The activity of H^+ ions in water is defined as $\{H^+\} = \gamma H^+ [H^+]$. Temperature and salinity exert opposing influences on ion activity, and thus pH. Increasing temperatures increase ion activity with a subsequent decrease in pH, while an increase in salinity results in reduced ion activity and increased pH (Zeebe & Wolf-Galdrow, 2001).

2.4 Partial Pressure of CO_2 (pCO_2)

The partial pressure of CO_2 is quantified by measuring the mole fraction of the gas and the total pressure of the gaseous mixture (P). The mole fraction of CO_2 (xCO_2) is proportional to the partial pressure: $pCO_2 = P * (xCO_2)$. An empirical relationship between temperature and pCO_2 indicates a 4% increase in pCO_2 associated with a 1°C change in temperature (Takahashi et al., 2002).

2.5 Saturation State of Aragonite (Ω)

The two major calcium carbonate minerals produced by marine organisms include calcite and aragonite. These minerals are secreted as shells and skeletons by many organisms including oysters, corals, and coccolithophorids. The carbonate saturation state (Ω) is defined as the product of calcium ion ([Ca^{2+}]) and carbonate ion concentrations divided by the stoichiometric solubility product (K_{sp}) at *in situ* conditions of salinity, pressure, and temperature (Zeebe & Wolf-Galdrow, 2001):

$$\Omega = \frac{[CO_3^{2-}][Ca^{2+}]}{K_{sp}} \qquad \text{Eq. 5}$$

Waters with $\Omega > 1$ are supersaturated, and the formation of $CaCO_3$ is thermodynamically favored; when $\Omega < 1$, waters are undersaturated, and dissolution of $CaCO_3$ may proceed.

3. Methods

3.1 Field Methods

The mainstem of the Chesapeake Bay is monitored monthly in the cooler months and twice monthly in the warmer months (May to September) at 49 stations by the Chesapeake Bay Water Quality Monitoring Program (CBMP; Chesapeake Bay Program, 2012). At each station, 19 parameters are routinely measured to assess water quality. For a full list of the parameters measured by the CBMP, refer to Chesapeake Bay Program, 2012). The Maryland (MD) portion of the CB is monitored by Maryland Department of Natural Resources (MD DNR), while Virginia's (VA) portion is monitored by Virginia Department of Environmental Quality (VA DEQ), in collaboration with Old Dominion University (ODU). Discrete samples of DIC and TA were collected at 17stations in conjunction with four routine CBMP sample collection cruises from 2016 to 2017: autumn (14 to 16 November, 2016); winter (14 to 17 February, 2017); spring (8 to 11 May, 2017); and summer (10 to 17 July, 2017). Riverine discharge from the Susquehanna, Potomac, and James Rivers during the 2016/2017 year was normal with maximum discharge observed during the spring season; i.e., the observations presented here were not collected in a particularly wet, or particularly dry year (United States Geological Survey, 2018).. The maximum depth of each station ranges from 4-32 meters. See Table 1 for specific cruise information and Table 2 for individual station information.

At each station, samples were collected 1 meter below the surface and 1 meter above the bottom, as well as at two intermediate depths depending on station depth and depth of the mixed layer. Density profiles were computed at each station as a function of temperature (T), salinity (S), and pressure (P) measured by the CBMP. The mixed-layer depth (MLD) was estimated using a percentage threshold, where stratification is assumed to occur if there is a change on the order of 10% of the difference between the maximum and minimum values of the density profile observed within one meter (Irby et al., 2016). Therefore, the MLD is defined as the shallowest occurrence (below 1-meter depth) where this percentage threshold is observed.

Onboard the MD DNR vessel, R/V Kerhin, discrete samples were collected using a Dayton 10 GPM submerged well pump. In VA waters, discrete samples were collected using a SeaBird 32 Mini-rosette with 12, 5-liter Ocean Test Equipment Go-Flo bottles onboard the ODU vessel, R/V Fay Slover. In both states, a YSI 6820 was used to measure temperature, salinity, DO, and pH at 1 to 2-meter resolution depending on station depth. From herein, pH measured by the CBMP sensors will be referred to as pH_{MP} to distinguish it from pH calculated using methods described below.

Discrete samples of DIC and TA were collected in 250-mL borosilicate bottles. Samples collected in VA were fixed using a saturated solution of mercuric chloride ($HgCl_2$) immediately after collection, then stored in the dark to await analysis. Samples collected in MD were immediately stored on ice in the dark and poisoned 2-6 hours after collection, as $HgCl_2$ was not permitted onboard the R/V Kerhin. To quantify the impact of delayed $HgCl_2$ addition, duplicate samples were collected in VA. Of the duplicates, one was treated with $HgCl_2$ immediately, the other was stored on ice and treated after 6 hours. The

difference in DIC concentrations between duplicate samples were indistinguishable from the uncertainty (3 μmol kg^{-1}). After each cruise, samples were returned to the Virginia Institute of Marine Science (VIMS) for further laboratory analysis.

3.2 Laboratory Methods

DIC concentrations were measured using a non-dispersive infrared (NDIR) analyzer (Airica by Marianda). NDIR gas analysis is an effective and fast technique for extracting and measuring concentrations from an acidified sample of seawater. During sample analysis, 2 mL of sampled seawater is extracted by a syringe and pumped into a stripping chamber where a dose of phosphoric acid (H_3PO_4) is added. A carrier gas (CO_2-free nitrogen) is then added to the stripping chamber at a constant rate and CO_2 is stripped out of the seawater sample. After extraction, water was removed from the gas via three drying mechanisms. First, the sample entered the condenser, where the Peltier cooler reduced the temperature to 4°C to remove water vapor from the sample. The sample then entered the inner, water permeable layer of Nafion tubing and air, dried by Drierite, circulated the outer layer of tubing in a countercurrent to completely dry the sample. The dry gas stream was then delivered to the NDIR sample cell (Li-COR, Li-7000). This process was completed three times per sample, resulting in just over 6 mL of sample used. The three sample peaks were integrated and two were averaged to determine the concentration of CO_2 from each sample.

TA concentrations were measured using an open-cell potentiometric titration with a system of components from Metrohm. A peristaltic pump was used to supply a known volume of sample seawater to a burette. The burette was then emptied into the titration cell

that had a recirculating water jacket that was maintained at 25°C. The titration cell contained a glass pH electrode, a thermometer, and a capillary tube that supplied acid to the sample. Once in the titration cell, hydrochloric acid was delivered to the sample by a computer-controlled piston burette. The titration process required two steps. The first step involved a single aliquot of acid that brought the sample to a pH between 3.5 and 4.0. Next, the solution was stirred, using a small magnetic stir bar within the titration cell, to allow CO_2 to escape the titration cell. While stirring, the titration continued as small increments of acid were added to the sample until a pH of 3 was reached. The acid used in these analyses was provided by A. G. Dickson (Scripps Institute of Oceanography) and produced in a solution of 0.6 mol kg^{-1} sodium chloride, which was used to approximate the ionic strength of seawater. When a pH of 3 was attained, following sufficient acid addition, the titration ended and a modified Gran approach was used to calculate the total alkalinity (Dickson et al., 2007).

For both the DIC and TA measurements, analysis of Certified Reference Materials (provided by A. G. Dickson, Scripps Institute of Oceanography; Batch #150) ensured an uncertainty of DIC and TA on the order of 3 μmol kg^{-1}. Following the determination of mainstem DIC and TA concentrations, the CO2SYS program (van Heuven et al., 2011) was used to compute pH using the total scale, pCO_2, and Ω with DIC and TA concentrations as input parameters. At each depth that a discrete sample of DIC or TA was collected, discrete concentrations of silicate and phosphate measured by the CBMP were used as input parameters in CO2SYS (Olson et al., 2012). The equilibrium constants of Mehrbach (1973) refit by Dickson & Millero (1987) and the KSO_4 constant of Dickson were used in this analysis. Tables 3 and 4 show the mean seasonal concentrations of DIC

and TA from each region from the mixed layer and subsurface waters, respectively, as well as the seasonal average of pH, Ω, and pCO_2, which were computed using DIC and TA as input parameters in CO2SYS.

3.3 Assignment of Geographic Regions

To reflect the natural, spatial variability in hydrographic and biogeochemical parameters throughout the CB, the mainstem was divided into four regions (Figure 3, Table 2) based on surface salinity (Figure 4). The northern region in the CB mainstem, Region 1 (R1), encompasses the deep oligohaline (S = 0.5 – 5) portion of the channel of the mainstem, where seasonal stratification is present after large freshwater inputs in the spring and summer. Region 2 (R2) is unique as its salinity regime seasonally shifts from mesohaline in the spring and summer (S = 5 – 18) to polyhaline (S > 18) in autumn and winter. Maximum station depth in both R1 and R2 was 32 meters. Within R2, sampling was oriented towards the deep channel in the western portion of the region. The most southern region was divided longitudinally due to the circulation pattern in the lower CB. As more saline ocean waters enter the mouth of the CB, they flow north along the Eastern Shore of VA where the mainstem is deeper and has decreased freshwater inputs (R3E; Goodrich & Blumberg, 1991). In this region, maximum station depth was 16 meters. Stations in the western half of the lower CB (R3W) receive greater freshwater inputs from the James, York, and Rappahannock Rivers with a maximum station depth of 11 meters. We assume that the observations used here are representative of each region (see section 4.1 and Table 5 for regional areas), yet recognize that the uneven spatial distribution of stations will result in uncertainty in measured and derived parameters in each region

Discrete samples were collected from two additional stations (CB1.1 and CB2.2) in autumn, spring, and summer in the northern CB near the mouth of the Susquehanna River. These stations are included in what will be referred to as R0 and are located upstream of R1. The TA and DIC data collected in this region are not included in further regional analysis due to their low salinity values and the large uncertainty associated with the equilibrium constants used in this analysis. The station at the mouth of the Susquehanna River, station CB1.1, has a salinity of 0 regardless of season, and salinity at station CB2.2, just south of the mouth of the Susquehanna River, is 0 in spring and summer and reaches a maximum salinity of 6 in autumn. Winter data were not collected at these stations by VIMS or the CBMP. Based on the seasonal salinity observations, these stations are heavily influenced by discharge from the Susquehanna River. Streamflow is comprised of baseflow (groundwater) and surface water runoff (stormwater). For example, at Conowingo, baseflow can typically comprise the majority of the flow (57%, Bachman et al., 1998).

The equilibrium constants used for DIC and TA measurements in this study (refer to section 3.2) are the conventional constants used for marine samples and have been used in other coastal CO_2-system studies (e.g., Shadwick et al., 2011; Xu et al., 2017; Jiang et al., 2010; Laurent et al., 2017). The constants of Mehrbach et al., (1973) refit by Dickson and Millero (1987) are best used for waters with temperature ranging from 2 – 35 °C, and from salinity ranging from 20 – 40, thus capturing many of the hydrographic characteristics of the mainstem waters, but not the characteristics of riverine waters from the CB watershed. Therefore, the CO_2-system measurements and calculations from R0 where the maximum salinity reaches 6 in only one season will have a much greater uncertainty than regions with higher salinities, and thus are not included in further regional partitioning.

3.4 Estimation of Total Alkalinity During the Winter Season

DIC and TA samples were collected during the winter season in the upper CB, but were not collected from the VA portion of the CB during the February (winter) cruise. We used the following procedure to estimate the missing winter values: First, a relationship between TA and salinity was derived using all available measurements of TA from samples collected between June 2016 and January 2018 (Figure 5a). Additional observations outside seasons included in this analysis are used to generate the most robust relationship between TA and S. Second, winter TA values were computed with (see Figure 5a):

$$TA_{winter} = 39(S) + 966 \qquad \text{Eq. 6,}$$

where TA_{winter} is the computed TA concentration in units of μmol kg^{-1} at a given salinity. The intercept value, 966 μmol kg^{-1}, in Eq. 6 indicates the concentration of TA in the Susquehanna River, the largest freshwater endmember in the CB system. Linear regression analysis (n=505, R^2=0.96, p<0.001) of all TA and corresponding salinity observations found a concentration of 966 μmol kg^{-1} to be the best fit in S=0 waters, with an uncertainty of 7 μmol kg^{-1} based on the standard error of the regression (Figure 5a). Finally, winter DIC, pCO_2 and Ω were computed using CO2SYS with TA_{winter} and pH_{MP} as described above. The computed DIC follows the relationship with salinity (Figure 5b).

3.5 Air-sea CO_2 flux

The air-sea CO_2 flux (F) was computed using the following equation:

$$F = k a \Delta pCO_2, \qquad \text{Eq. 7}$$

where k is the gas transfer velocity (m s^{-1}) calculated using the formulation of Wanninkhof (2014) for intermediate wind speeds (3–15 m s^{-1}), *a* is the solubility coefficient of CO_2 (Weiss, 1974), and ΔpCO_2 is the gradient of CO_2 between the ocean and the atmosphere ($\Delta pCO_2 = pCO_2^{air} - pCO_2^{ocean}$). The flux is given in units of mmol m^{-2} day^{-1}. When F is positive, there is a CO_2 flux from the atmosphere to the surface waters. Wind speeds were obtained at a height of 4 meters above the surface water from three buoys in the Chesapeake Bay Interpretive Buoy System (CBIBS; https://buoybay.noaa.gov) at a height of 4 m above the water surface: the Gooses Reef Buoy in R1, the Potomac Buoy in R2, and the York Spit Buoy in R3E and R3W. The York Spit Buoy is located in R3W, but the wind speed from this location was used for R3E as well due to an incomplete record of windspeed in R3E for the period of observation. The average wind speed over the entire cruise duration was used (i.e., spring cruise was 4 days) (Tables 1, 5). The atmospheric CO_2 used in this study is the 2016 annual average, 405.6 μatm, from the World Data Center for Greenhouse Gases station in Key Biscayne, Florida. The regional fluxes were found by computing the flux at each station in each region then averaging over all the stations in a particular region. These regional fluxes were then scaled to the surface area of each region. The surface areas of each region were determined using Chesapeake Bay Program (2004) segment CB4MH, encompassing the northern deep channel of R1, segment CB5MH corresponding to the western middle Bay where samples were collected in R2, segment CB6PH and half of CB8PH corresponding to R3W, and segment CB7PH and half of CB8PH encompassing the surface area of R3E. The sum of the area-weighted fluxes in each season were used to determine the annual source/sink status of atmospheric CO_2 in the CB mainstem.

3.6 Mass Balance of DIC

The total change in DIC concentration per unit time (ΔDIC_{total}) is equal to the sum of the changes due to biological drivers (photosynthesis and respiration (ΔDIC_{bio}), and biogenic calcification) and physical drivers (air-sea CO_2 exchange (ΔDIC_{gas}), horizontal and vertical mixing (ΔDIC_{circ}), and calcium carbonate ($CaCO_3$) dissolution). Due to the conservative behavior of TA as a function of salinity (Eq. 6), we assume that calcification and dissolution of $CaCO_3$ can be neglected (Figure 5a). In the mixed layer, the temporal change in DIC concentrations between seasons (in units of μmol kg^{-1} $month^{-1}$) can thus be expressed as:

$$\Delta DIC_{total}^{ML} = \Delta DIC_{bio}^{ML} + \Delta DIC_{circ}^{ML} + \Delta DIC_{gas}^{ML} \quad \text{Eq. 8}$$

In subsurface waters, the seasonal changes in DIC can be expressed as:

$$\Delta DIC_{total}^{sub} = \Delta DIC_{bio}^{sub} + \Delta DIC_{circ}^{sub} \quad \text{Eq. 9}$$

DIC_{total}^{ML} and DIC_{total}^{sub} were computed by first determining the average concentration of DIC in the mixed layer and subsurface waters, respectively, (in units of μmol kg^{-1}) from all stations in a region in a given season. ΔDIC_{total}^{ML} and ΔDIC_{total}^{sub} were computed as the difference of the mean DIC concentrations above and below the mixed layer, respectively, in each region divided by the time in months between seasons. The change in time (Δt) between autumn and winter and winter and spring was three months and Δt between spring and summer was two months. Between summer and autumn, there is assumed to be no change in DIC. ΔDIC_{gas}^{ML} was computed from the difference of the seasonal air-sea CO_2 flux divided by the seasonal mixed layer depth in each region (Table 3). ΔDIC_{circ}^{ML} and ΔDIC_{circ}^{sub} were calculated via the expected DIC for a particular salinity (DIC_{sal}), based on

a regression of DIC and salinity using all samples collected between June 2016 and January 2018 (Figure 5b):

$$DIC_{sal} = 34(S) + 973 \qquad \text{Eq. 10}$$

where DIC_{sal} has units of μmol kg^{-1}. DIC_{sal} was computed at each station during all seasons. The change in the mean DIC_{sal} from all stations in a given region between seasons was then assumed equal to ΔDIC_{circ}^{ML} and ΔDIC_{circ}^{sub}, in the mixed layer and subsurface waters, respectively. Finally, the contribution from biological processes in the mixed layer (ΔDIC_{bio}^{ML}) and subsurface waters (ΔDIC_{bio}^{sub}) were computed by difference. In the mixed layer (Eq. 11) and subsurface waters (Eq. 12), the contributions from biological processes were defined as:

$$\Delta DIC_{bio}^{ML} = \Delta DIC_{total}^{ML} - \Delta DIC_{circ}^{ML} - \Delta DIC_{gas}^{ML} \qquad \text{Eq. 11}$$

$$\Delta DIC_{bio}^{sub} = \Delta DIC_{total}^{sub} - \Delta DIC_{circ}^{sub} \qquad \text{Eq. 12}$$

In the northern CB regions (R1 and R2), all stations contain both mixed layer and subsurface values in each season. In R3E, there are stations that are well-mixed throughout the water column in certain seasons (e.g., winter), but stratified in other seasons (e.g., summer). In R3W, there are both stations that are well mixed in each season and stations that experience stratification. In R3W, the autumn, winter, and summer subsurface budgets are based on observations from a single station; the spring subsurface budget is based on observations from two stations. In R3E, the autumn subsurface budget is based on observations from a single station, as all other stations are well mixed and therefore included in the mixed layer budget. The sum of the mixed layer and subsurface values are used to generate whole water column values of ΔDIC_{bio} (ΔDIC_{bio}^{full}) and subsequently net community production. To convert from concentration of DIC (μmol kg^{-1}) in the mixed

layer and subsurface waters to units of mol C m^{-2} $month^{-1}$, the average seasonal density in each region is needed, along with average depth of the mixed layer and subsurface layer in each region during each season.

3.6 Uncertainty Analysis

Because ΔDIC_{bio} is computed by difference, the uncertainty of this term includes the uncertainty associated with each of the other terms in Eqs. 11 and 12. The uncertainty associated with ΔDIC_{total} in both the mixed layer and subsurface waters is small (2 μmol kg^{-1}) and based on the analytical uncertainty of the measurement. The uncertainty associated with ΔDIC_{gas}^{ML} was estimated from the standard deviation of the flux computed via three different parameterizations of the gas transfer velocity: Wanninkhof (2014), Wanninkhof & McGillis (1999), and Nightingale et al., (2000), and is on the order of 5 μmol kg^{-1}, corresponding to 0.03 mol C m^{-2} $month^{-1}$ (assuming a mean mixed layer depth of 5.4 meters and a mean density of 1013 kg m^{-3}). The uncertainty associated with DIC_{circ} is estimated to be 12 μmol kg^{-1}, determined from the standard error of the regression between DIC and salinity (Eq. 10, Figure 5b). The resulting uncertainty associated with the ΔDIC_{bio} in the mixed layer (13 μmol kg^{-1}) and subsurface waters (12 μmol kg^{-1}) was computed by propagating the errors associated with all other terms (i.e., $(3^2+5^2+12^2)^{1/2}$ for the mixed-layer) and assuming that the errors are uncorrelated.

4. Results

4.1 Representativeness of Mainstem Cruises

From the long-term (1984 – 2017) CBMP climatology in each region, it is clear that the four 2016/2017 cruises included in this analysis are representative of the broad hydrographic seasonality in the CB mainstem, with few observed values outside the range of the long-term data (Figure 6). Throughout the CB mainstem, waters exhibit a pronounced seasonality in surface temperature (SST; seasonal range on the order of 30 ^{o}C, Figures 6a, c, e, g). Temperature in all four regions ranged from less than 5 ^{o}C in winter to greater than 25 ^{o}C in summer. Seasonality in salinity shows maximum values in winter and some degree of freshening in the spring and summer seasons across all regions (Figures 6b, d, f, h).

4.2 Seasonality of CO_2-system Parameters Throughout the Mainstem

The seasonality of the CO_2-system is influenced by both hydrographic (i.e., changes in temperature and salinity) and biological (i.e., photosynthesis and respiration) drivers, as well as the air-sea exchange of CO_2, with different parameters exhibiting differing sensitivity to these changes. In this section, the seasonality of DIC, TA, pH, Ω, and pCO_2 in both the mixed layer and subsurface waters will be described (Tables 3, 4); the seasonality of temperature-normalized pCO_2 (pCO_2^{Tmean}) and air-sea CO_2 fluxes are described in the next section.

It is important to understand the seasonal variability of both DIC and TA concentrations in R0 before looking further down the mainstem. The seasonality of TA and DIC concentrations in S = 0 waters ranges from 650–1300 μmol kg^{-1} and 700–1300 μmol kg^{-1},

respectively. During periods of low riverine discharge, particularly in late summer and early autumn, concentrations of TA are elevated (Figure 7). Despite the higher concentrations of TA and DIC delivered to R0 during low flow periods, the overall TA and DIC load is greater in the spring, corresponding to a seasonal increase in freshwater discharge from the Susquehanna River. This characteristic of a mainstem tributary is different than the mainstem itself, where enhanced freshwater influx corresponds to reduced TA and DIC concentrations, driven by the decline in salinity (see section 4.4).

Throughout and below the mixed layer, there is very little variability in temperature between regions and each region experiences the same large range in temperature over the course of the year (Figures 8a, 9a). The observed spatial and seasonal variability of salinity depicts the expected seasonality in streamflow, where there is a smaller seasonal range in salinity in the southern regions of the mainstem when compared to northern regions as a result of the reduced freshwater input to the lower CB (Figure 8b). This is particularly evident in the mixed layer, where the regions with greatest freshwater input have the largest seasonality in salinity. This spatial trend is observed in subsurface waters as well, yet the seasonality in the upper mainstem regions are reduced when compared to the mixed layer (Figure 9b). The seasonality of DIC and TA in both the mixed layer and subsurface waters almost perfectly mimic that of salinity in each region, as expected (Figures 8a, b, c). Minimum concentrations of DIC and TA were observed in the northern CB, with mixed layer minimum concentrations of 1000 μmol kg^{-1} and full water column minimum concentrations of 1500 μmol kg^{-1}. Maximum concentrations of DIC and TA were observed at the mouth of the CB, with mixed layer maxima on the order of 1800 μmol kg^{-1} and 1900

μmol kg^{-1}, respectively, and subsurface maximum concentrations on the order of 1900 μmol kg^{-1} and 2000 μmol kg^{-1}, respectively (Figures 8c, d, 9c, d).

There is large variability in both pH and Ω throughout and below the mixed layer. The highest pH values were observed during the cool months (Figures 8e, 9e). In the mixed layer, a pH maximum was observed during autumn in R1 and R3E and a pH maximum was observed during winter in R2 and R3W. There is a change in temperature of 8.2 °C in the mixed layer of R2 between autumn and winter. Assuming DIC, TA, S, and T remain constant, this change in temperature would result in an increase in pH of about 0.13, but as this large of an increase is not observed, it is clear there are other processes acting to drive pH seasonality (Figures 8e, 9e). Below the mixed layer, each region except R1 exhibited the highest pH in winter coincident with minimum temperature. Throughout the subsurface waters of R1, there is a seasonal decline in pH over the course of the year, which is coincident with the onset of seasonal stratification and an increase in respiration throughout the water column as temperature increases. The seasonality of pH in the mixed layer of R1 is similar to that of Ω in both the mixed layer and whole water column, with lowest values in winter and spring. The seasonal cycle of Ω in the mixed layer is similar in each region of the mainstem (Figure 8f). Over the course of the year, the mixed layer of the CB is supersaturated with respect to aragonite, except in R1 where undersaturation of Ω occurs in winter and spring. The subsurface waters in R1 are undersaturated with respect to Ω in each season except autumn, and R2 is undersaturated during the warm seasons, and nearly undersaturated in winter. The shallow regions of the lower CB that directly exchange with the Atlantic Ocean are supersaturated with respect to Ω over the course of the year (Figures 8f, 9f).

In the mixed layer of the two northern mainstem regions, pCO_2 is undersaturated in each season, whereas the mixed layer in the lower CB experiences seasonal supersaturation with respect to atmospheric CO_2 during the warm seasons (Figures 8g, 9g). Below the mixed layer, pCO_2 is generally supersaturated over the seasonal cycle, particularly during the warm seasons in R1 and R2 (Figures 8g, 9g). The difference between the mixed layer and subsurface waters is presumably driven by the accumulation of CO_2 below the mixed layer during periods of seasonal stratification in the upper mainstem. There is a significant seasonal range in pCO_2 in each region, with values varying by over 100 μatm between seasons in the mixed layer and 1300 μatm between seasons below the mixed layer. The seasonal cycle of pCO_2 varies regionally, with mixed layer minimum values on the order of 170 μatm and maximum values on the order of 450 μatm. Minimum pCO_2 in subsurface waters is 260 μatm and maximum values reach 2800 μatm (Figures 8g, 9g). In contrast to the varying seasonal cycle of pCO_2 in the mixed layer of each region, the complete seasonal cycle of pCO_2 is the same in the subsurface waters in all regions, with highest values observed in summer (Figures 8g, 9g). The pronounced SST seasonality in the CB has an important influence on pCO_2. This influence is further demonstrated by the large differences between pCO_2 (Figures 8g, 9g) and pCO_2^{Tmean} (Figures 8h, 9h).

4.3 Temperature-normalized pCO_2 and Air-sea CO_2 Fluxes

To examine the non-thermal contributions to pCO_2 seasonality, observations were normalized to the annual mean temperature (T_{mean} = 16 °C) via the equation of Takahashi et al. (2002):

$$pCO_2^{Tmean} = (pCO_2)_{obs} \times \exp[0.0423\ (T_{mean} - T_{obs})] \qquad \text{Eq. 13}$$

where 'obs' indicates the *in-situ* pCO_2 and temperature.

The seasonal range in pCO_2^{Tmean} can be as large as 200 μatm in the mixed layer and 1100 μatm in subsurface waters, indicating significant non-thermal impacts to pCO_2 seasonality in the CB mainstem (Figures 8h, 9h). Throughout the mixed layer and in subsurface waters, there is an increase in pCO_2^{Tmean} from autumn to winter in each region, which is presumably driven by an increase in CO_2 as a result of respiration. In the mixed layer, an ingassing of atmospheric CO_2 contributes to this seasonal increase as well. In R1 and R3E, this increase in pCO_2^{Tmean} from autumn to winter was coincident with increased concentrations of DIC (Figures 8c, h) — this will be explored in more detail in section 4.4. In the mixed layer, a decrease in pCO_2^{Tmean} from winter to spring and from spring to summer is observed in each region. This decrease in mixed layer pCO_2^{Tmean} was likely a result of the net removal of CO_2 via biological productivity during these seasons, as well as occasional seasonal outgassing of CO_2 from the surface waters to the atmosphere (Figure 8h). In the subsurface waters, there was a large increase in pCO_2^{Tmean} from winter to spring, and again from spring to summer in the deep regions, R1 and R2 (Figure 9h). A smaller increase in subsurface pCO_2^{Tmean} was observed from winter to summer in R3W. These increases were likely driven by the accumulation of CO_2 in subsurface waters during the warmer seasons in the CB mainstem. Similar to the seasonality in the mixed layer, there was a decrease in pCO_2^{Tmean} in the subsurface waters of R3E from winter to summer presumably driven by the removal of CO_2 through biological processes (Figure 9h).

The surface waters in R1 are undersaturated with respect to the atmosphere in all seasons and the region was a net sink on the order of 3.7 mol C m^{-2} yr^{-1} (Figure 10). The undersaturation of pCO_2 with respect to the atmosphere in R2 over the course of the year

similarly results in an uptake of CO_2 on the order of 2.2 mol C m^{-2} yr^{-1}. Although R3W was modestly supersaturated with respect to the atmosphere in the summer season, the region acts as a net sink of 0.76 mol C m^{-2} yr^{-1}. Surface waters in R3E are supersaturated with respect to the atmosphere during both spring and summer, however, the region acts as a net sink on the order of 0.42 mol C m^{-2} yr^{-1}. When scaled to the surface area of the mainstem (Table 5), these waters act as sink for atmospheric CO_2 on the order of 1.6 mol C m^{-2} yr^{-1}.

4.4 Seasonal Mass Balance of DIC

The seasonal change of DIC observed in the surface mixed layer of the CB mainstem was driven by gas exchange, circulation, and biological processes with the seasonal changes from circulation and biology often dominating (Table 6, Figure 11). Throughout the mainstem, the ΔDIC_{gas}^{ML} term was positive for most of the year, indicating an increase in mixed layer DIC concentrations as a result of the invasion of atmospheric CO_2. As shown in the previous section, each region of the mainstem acts as a net sink of atmospheric CO_2, despite the periods of seasonal outgassing in the lower CB regions (Figures 11c, d). ΔDIC_{circ}^{ML} is net negative over the complete seasonal in the mixed layer of each region, indicating a net loss of DIC driven by a reduction in salinity from autumn to summer. In each region of the mainstem from winter to spring, the net loss of DIC from the mixed layer from ΔDIC_{circ}^{ML} is expected as there is a large increase in streamflow during this seasonal transition (Figure 11). This decline in DIC from ΔDIC_{circ}^{ML} is particularly evident in R1 where the net removal of DIC from the mixed layer is driven by increased Susquehanna River streamflow, as well as the removal of DIC from ΔDIC_{bio}^{ML} as a result

of the onset of the spring phytoplankton bloom (Figure 11a). The ΔDIC_{bio}^{ML} term is almost always negative, indicating a net loss of DIC through biological processes in the mixed layer of each region over the course of the year. The less frequent conditions of positive ΔDIC_{bio}^{ML}, indicating a source of DIC from respiration or remineralization, are concurrent with outgassing of CO_2 from the surface waters and occur only in the shallow regions of the lower CB during the warm seasons (Figures 11c, d).

In the subsurface, changes in DIC are driven by circulation and biology with contributions from ΔDIC_{circ}^{sub} dominating in most seasons (Figure 12). Unlike the surface mixed layer, the ΔDIC_{bio}^{sub} term is positive in every region and season, with the exception of the transition from spring to summer in R3E (Figure 12d). This is indicative of the dominance of respiration in the subsurface waters. The positive ΔDIC_{bio}^{sub} is much greater in R1 and R2 than the lower CB regions due to the stratification that occurs in the deep, northern CB that prevents ventilation of subsurface waters (Figures 12a-d). ΔDIC_{circ}^{sub} is always negative from winter to spring, indicating a net removal of DIC driven by seasonality in riverine inputs. In the upper bay, ΔDIC_{circ}^{sub} was net negative over the complete seasonal cycle in both regions, while in the lower bay, increases in salinity, corresponding to reduced riverine inputs, drove net increases in DIC in the subsurface waters (i.e., $\Delta DIC_{circ}^{sub} > 0$) throughout the year (Figure 12).

4.5 Net Community Production

Net community production (NCP) is defined as the difference between net primary production (NPP) and heterotrophic respiration (HR):

$$NCP = NPP - HR, \qquad \text{Eq. 15}$$

And is equal to the net biologically driven changes of DIC (i.e., NCP = $\Sigma\Delta DIC_{bio}$) resulting from the mass balance of DIC described above. Over the seasonal cycle analyzed here, the mixed layer of all regions in the CB are net autotrophic (i.e., $\Delta DIC_{bio}^{ML} < 0$; Table 6) indicating that primary production dominated heterotrophic respiration and resulted in an overall net biological consumption of DIC in the surface mixed layer (Table 7). In both R1 and R2 (e.g., upper and mid CB) the mixed layer was autotrophic (Figures 11a, b). In R3W, heterotrophic conditions are observed between spring and summer, but the region was net autotrophic (Figure 11c). Here, seasonally varying conditions of both autotrophy and heterotrophy have been observed (Shadwick et al., in revision). In R3E, the surface mixed layer was heterotrophic from winter to spring, and autotrophic for the remainder of the study period. Overall, the mixed layer of the mainstem was autotrophic. The sum of the seasonal mixed layer NCP from each region (Table 7) scaled to the region's surface area (Table 5), results in a mainstem NCP of 1.2 ± 0.1 mol C m^{-2} $year^{-1}$ (± with the error estimated from the uncertainty of the ΔDIC_{bio} terms). When considering the whole water column, each region was net heterotrophic during the study period (Fig. 8e). Using the same method described above, the whole water column had an annual NCP of -0.48 mol C m^{-2} $year^{-1}$.

5. Discussion

5.1 *Net Community Production in the Context of Earlier Estimates*

Kemp et al. (1997) found distinct patterns in mainstem NCP using data form 1986 – 1993 that differ from the regional variability presented here. Although the regional division of the CB mainstem used by Kemp et al. (1997) is different from this study, their "mid-Bay" corresponds to our R1 and R2, and their "lower Bay" corresponds to our R3W and R3E. The tidal freshwater region used by Kemp et al. (1997) encompassed the low-salinity and high-turbidity zone near the mouth of the Susquehanna River and was not included in this study. This region, as well as the upper regions of CB tributaries, is often heterotrophic (e.g., Raymond et al., 2000) as a result of light limitation for primary production (Reay, 2009; Sin et al., 1999) and large amounts of bacterial respiration (Schultz, 1999). The inclusion of these low-light, high-turbidity zones in the upper CB of Kemp et al. (1997) contribute to their net heterotrophic findings in this region. The mid-CB of both Kemp et al. (1997) and the corresponding area of the mainstem mixed layer in this study (R1 and R2) were net autotrophic, whereas the whole water column in these regions were net heterotrophic. The annual value computed by Kemp et al. (1997) for this region was 13.6 ± 2.5 g C m^{-2} yr^{-1}, whereas the sum of the values of the complete seasonal cycle in the mixed layer of R1 and R2 is 51.6 ± 1.2 g C m^{-2} yr^{-1} and the whole water column was -23.3 ± 1.2 g C m^{-2} yr^{-1} (Table 6). In contrast to the results of Kemp et al. (1997), we found that mixed layer of the lower CB regions were less autotrophic than R1 and R2 and that the whole water column was net heterotrophic. However, this is likely driven by the reduction in nutrient loading to the mainstem since the study by Kemp et al. (1997) and due to the inclusion of multiple shallow stations in the lower Bay of this study compared to those

used by Kemp et al. (1997). The mixed layer of the lower CB in this study did experience net heterotrophic conditions in particular seasons (Figure 7c, d). A major similarity between the findings of this study and that of Kemp et al. (1997) is the period of heterotrophy in the mixed layer of the lower CB (R3E in this study; Figure 7d) from winter to spring, despite the region being net autotrophic over the course of the year.

The 3D hydrodynamic-biogeochemical modeling study of Feng et al. (2015) found the Chesapeake Bay to be net autotrophic. If we convert their NCP values to carbon units using a Redfield ratio of C:N = 106:16, the authors' annual average for 2001 – 2005 is $4.2 \times 10^{11} \pm 1.3 \times 10^{11}$ g C yr^{-1}. This is similar to our mixed layer estimate when it is scaled to a comparable surface area of Feng et al. (2015) that similarly includes both the tributaries and mainstem (1.3×10^{11} g C yr^{-1}). NCP was computed for 5 years in Feng et al. (2015). Over the five – year period examined by Feng et al. (2015), the NCP varied by an order of magnitude indicating that interannual variability, and not only seasonality, plays a large role in dictating the trophic status of a system. Finally, both Najjar et al. (2018) and Herrmann et al. (2015) classified the CB as net autotrophic, despite their conclusion that the majority of estuarine systems on the East Coast of the United States are heterotrophic. The results of this study, however, indicate that the whole water column of the CB mainstem during the 2016/2017 study period is net heterotrophic, therefore behaving more similarly to other East Coast estuaries.

5.2 *Comparison with Other Estuarine and Coastal Ocean Systems*

In this section, the observed variability of the CO_2 system in the CB is compared to recent work in the Chesapeake Bay and the neighboring Delaware Bay, as well as earlier

work in the North Sea, to give a broader perspective on how estuaries and other semi-enclosed systems fit into an emerging understanding of the coastal ocean carbon cycle. A recent study in the Chesapeake Bay by Brodeur et al. (2019) observed a similar latitudinal gradient in both DIC and TA throughout the mainstem and consistent concentrations of DIC. Regardless of season, higher pH was observed in the surface waters than at depth in both studies.

A recent modelling study computed the annual air-sea CO_2 flux from the CB mainstem surface waters. Shen et al. (2019) found regions R1 and R2 of this study to be net sinks of atmospheric CO_2, whereas the lower CB was in a net balanced condition. This spatial trend is similar to what is reported here, as the northern regions act as a strong sink of atmospheric CO_2 when compared to the lower CB regions, which are near neutral on the annual scale (Figure 10). We note that the annual air-sea CO_2 flux determined by Shen et al. (2019) included the tidal, freshwater region of upper CB, located north of R1 of this study, in their annual estimate. This region acts as a strong source of CO_2, as surface waters are supersaturated with CO_2 with respect to the atmosphere.

The Delaware Bay is a large estuary located just to the north of the CB along the US East Coast. The region has a similar latitudinal gradient in salinity to that of the CB and recent studies have characterized the CO_2-system in this estuary (Joesoef et al., 2017; Joesoef et al., 2015). When comparing R1 in the CB to the Delaware Bay estuarine zone defined by Joesoef et al. (2017), the findings are quite different. This narrow region of the Delaware Bay is heterotrophic and has supersaturated surface waters with respect to atmospheric CO_2 on the annual scale, with values reaching over 2000 μatm during the summer season (Joesoef et al., 2015; Joesoef et al., 2017), in contrast to our findings that

R1 and R2 were undersaturated with pCO_2 with respect to the atmosphere over the entire seasonal cycle (Figure 8g). For the comparison of these two systems, the S = 0 waters at the head of the CB that are supersaturated with respect to atmospheric CO_2 are not included. To be consistent, the tidal freshwater zone, defined by Joesoef et al. (2017), was also not included; in this S = 0 region, surface pCO_2 values range from 950 μatm in spring to 4000 μatm in summer. According to Joesoef et al. (2017), the full water column in the lower Delaware Bay exhibits a similar seasonality to that of the mixed layer in R3W in this study. Throughout this region of the Delaware Bay, there was a large loss of DIC due to CO_2 consumption from winter to spring, followed by a period of heterotrophy from spring to summer (compare to Figure 11c). On the annual scale, the Delaware Bay was net heterotrophic, acting as a source of DIC, with an NCP of -1.3 mol C m^{-2} yr^{-1} (Joesoef et al., 2017). Additionally, when comparing these two systems, it is important to consider that the Delaware Bay does not experience the impacts of eutrophication like those observed in the CB, which is largely driven by the lack of seasonal stratification in the Delaware Bay (Sharp et al., 1982). The phytoplankton growth that is initiated after the introduction of excess nutrients to the surface mixed layer of the upper CB contributes to the reduction in surface water pCO_2 that is not observed in the surface waters of the Delaware Bay (Sharp et al., 1982).

While the North Sea is a semi-enclosed regional sea, and not an estuary, the consistency in the methods between the early work in the North Sea (Thomas et al., 2004; Bozec et al., 2006) and the current research in the Chesapeake Bay, along with similarities in seasonal and spatial variability, allow for a comparison between the two regions. R1 in the CB can be compared to the northern region of the North Sea, while R3W and R3E can be compared

to the southern region of the North Sea. The northern section of the North Sea reaches a maximum depth of 700 m and experiences seasonal stratification that results in large vertical gradients in biogeochemical parameters in spring and summer (Thomas et al., 2004). From winter to summer in the northern North Sea in 2002, Thomas et al. (2004) observed a depletion in DIC in the surface waters on the order of 100 μmol kg^{-1}. Over the same seasonal transition in this study, there was a surface depletion in DIC on the order of 500 μmol kg^{-1} in R1 of the CB mainstem. This surface depletion was concurrent with the onset of stratification in both systems (Thomas et al., 2004; Bozec et al., 2006). In the northern North Sea, the surface depletion can be attributed mainly to the drawdown of DIC through biological processes, whereas in R1 of the CB, it was attributed to a combination of biological processes and changes in estuarine circulation patterns (Thomas et al., 2004; see section 4.4). The subsurface DIC accumulation in both systems was driven by the remineralization of organic matter below the mixed layer and the lack of ventilation with the atmosphere. In both systems, large vertical gradients of DIC are observed in summer, on the order of 200 μmol kg^{-1} in the northern North Sea (Thomas et al., 2004; Bozec et al., 2006), and 700 μmol kg^{-1} in R1 in the CB.

By contrast, the southern portion of the North Sea can be compared to the region R3W in the lower CB of this study, as they are shallower than the northern regions and exhibit a similar seasonality in water column DIC (Thomas et al., 2004; Bozec et al., 2006). When the water column is well mixed, primary production and respiration may occur throughout the same compartment of the water column in the southern regions of both systems (Thomas et al., 2004). There was a seasonal deficit of less than 60 μmol kg^{-1} DIC from winter to spring in both the southern North Sea and R3W, concurrent with the initiation of

a spring phytoplankton bloom, followed by a gradual increase in the DIC from spring to summer as the respiration of organic matter dominates over the removal of DIC through photosynthesis (Bozec et al., 2006; Thomas et al., 2004). Throughout the year, both the entire North Sea and mixed layer of the CB mainstem are autotrophic, despite the seasonal and spatial variability in biologically driven changes to DIC throughout both systems.

Referring back to sections 3.2 and 3.3, a comparison of the seasonality of surface water pCO_2 in both the CB and North Sea can be made. The northern regions of the North Sea and the CB are undersaturated on average throughout the year and act as an annual sink of atmospheric CO_2, with a particularly strong removal of atmospheric CO_2 during spring and summer (Thomas et al., 2004; Thomas et al., 2005). The northern regions of the CB (R1 and R2) act as a sink of 2.8 mol C m^{-2} yr^{-1}, and the northern North Sea was a sink of 1.7 mol C m^{-2} yr^{-1} (Thomas et al., 2005). The lower CB regions and the southern North Sea experience seasonal supersaturation of the surface waters, particularly during the summer season (Figure 8g). During the summer in both systems, the increase in temperature, combined with enhanced CO_2 input from the remineralization of organic matter, drive the supersaturation of these surface waters (Thomas et al., 2004). While both systems act as a source of CO_2 to the atmosphere during the summer season, on the annual scale the two lower CB regions act as a total net sink of 0.54 mol C m^{-2} yr^{-1}, whereas the southern region of the North Sea acts as a weak source of 0.2 mol C m^{-2} yr^{-1} to the atmosphere (Figure 10; Thomas et al., 2004; Thomas et al., 2005). When considering the entire CB mainstem and North Sea, both systems act as considerable, and comparable, annual sinks of atmospheric CO_2, on the order of 1.6 mol C m^{-2} yr^{-1} and 1.4 mol C m^{-2} yr^{-1}, respectively (Thomas et al., 2005).

6. *Summary and Conclusions*

This study was one of the first to observe the variability of the CO_2-system throughout the entire CB mainstem over a complete seasonal cycle. Using 17 mainstem stations subdivided into four geographic regions, the seasonality of DIC, pCO_2, pH, and Ω were examined. Regardless of season, gradients of both DIC and TA were observed in the surface mixed-layer of the CB mainstem, with lowest concentrations observed in the northern CB near the mouth of the Susquehanna River and highest concentrations observed at the mouth of the CB where estuarine waters closely interact with Atlantic Ocean shelf waters. The accumulation of high-DIC waters at depth, coincident with seasonal stratification and temperature-dependent remineralization of organic matter, will exacerbate ocean acidification in this coastal system, as well as drive the undersaturation with respect to Ω and supersaturation of pCO_2 with respect to atmospheric values in these subsurface waters on the annual scale. In the surface waters of the stratified upper CB (north of the Potomac), pCO_2 is undersaturated with respect to the atmosphere year-round resulting from a dominance of the removal of CO_2 by photosynthesis over thermally driven changes in pCO_2. Conversely, surface waters in the lower CB experience seasonal CO_2 outgassing as the thermally driven increase in pCO_2 outweighs the biologically driven removal of DIC as the productive season declines. The CB mainstem was a net sink for atmospheric CO_2 on the order of 1.6 mol C m^{-2} yr^{-1}.

A mass balance of DIC was used to partition the seasonal changes in DIC into physical and biological drivers throughout the mainstem, and the annual uptake of atmospheric CO_2 was quantified. When scaled to the surface area of the mainstem, the results indicate that the mixed layer of the CB mainstem was net autotrophic in 2016/2017, with a net

community production of 1.2 mol C m^{-2} $year^{-1}$ and that the whole water column was net heterotrophic, with a net community production of -0.48 mol C m^{-2} $year^{-1}$ over the study period.

In the future, further analysis of how the seasonality of the CO_2-system in freshwater dominated regions influences biogeochemical cycling throughout the mainstem is needed. In the tidal freshwater tributaries of the CB, unique CO_2-system interactions between riverine inputs, consisting of baseflow and stormwater contributions and large areas of submerged aquatic vegetation may contribute to the delivery and seasonality of biogeochemical parameters from the freshwater endmember to the rest of the system, thus contributing to the natural variability experienced in this large estuary. Because interannual variability in this dynamic nearshore system is likely to be large, continued monitoring of CO_2-system parameters should be prioritized. As anthropogenic changes (i.e., as a result of increased atmospheric CO_2) to these waters are small compared to natural variability, the work presented here represents a crucial step in understanding the evolution of coastal systems in response to climate change.

Table 1. Dates and cruise ID of seasonal observations. The number of months (Δt) between autumn and winter = 3 months, winter and spring = 3 months, spring and summer = 2 months.

Start Date	End Date	Season	CBP cruise ID
November 14, 2016	November 16, 2016	Autumn	684
February 14, 2017	February 17, 2017	Winter	690
May 8, 2017	May 11, 2017	Spring	696
July 10, 2017	July 17, 2017	Summer	700

Table 2. Depth and location of each station used in this analysis.

Station	Region	Latitude (°N)	Longitude (°W)	Station Depth (m)
CB3.3C	R1	38.996	-76.360	24
CB4.1C	R1	38.826	-76.400	32
CB4.2C	R1	38.646	-76.421	27
CB4.4	R1	38.415	-76.346	31
CB5.2	R2	38.137	-76.228	31
CB5.4	R2	37.800	-76.175	32
CB5.5	R2	37.692	-76.190	17
CB6.3	R3W	37.412	-76.160	11
LE3.7	R3W	37.531	-76.307	6
WE4.1	R3W	37.312	-76.346	4
WE4.4	R3W	37.110	-76.293	4
CB7.1S	R3E	37.581	-76.058	16
CB7.2E	R3E	37.412	-76.025	12
CB7.3	R3E	37.117	-76.125	12
CB7.4N	R3E	37.062	-75.999	10
CB8.1	R3E	36.995	-76.168	8
CB8.1E	R33E	36.947	-76.035	14

Table 3. Mean values of mixed layer CO_2-system parameters in each region. The ± represents the standard deviation of the seasonal average of each parameter in the surface mixed layer in each region. n is the number of stations included when computing the average value in each season.

	DIC^{ML}	TA^{ML}	pH^{ML}	Ω^{ML}	pCO_2^{ML}	S^{ML}	T^{ML}	MLD	n
Units	μmol kg^{-1}	μmol kg^{-1}			μatm		°C	m	
R1									
Autumn	1364 ± 95	1520 ± 69	8.5 ± 0.1	1.83 ± 0.3	169 ± 59	16.2 ± 1.8	13.5 ± 0.4	3.3 ±1.5	3
Winter	1484 ± 26	1547 ± 35	8.3 ± 0.1	0.84 ± 0.1	245 ± 11	15.5 ± 1.0	4.8 ± 0.3	7.3 ± 3.8	3
Spring	1033 ± 82	1076 ± 91	8.3 ± 0.04	0.69 ± 0.1	229 ± 26	5.3 ± 2.5	17.2 ± 0.4	5 ± 2.6	3
Summer	1196 ± 51	1316 ± 48	8.4 ± 0.1	1.73 ± 0.6	193 ± 82	9.3 ± 1.5	27.1 ± 0.4	9.3 ± 2.9	4
R2									
Autumn	1633 ± 7	1753 ± 13	8.2 ± 0.01	1.44 ± 0.1	307 ± 9	20.0 ± 0.5	13.7 ± 0.1	4.5 ± 0.7	2
Winter	1585 ± 12	1682 ± 21	8.3 ± 0.03	1.16 ± 0.1	232 ± 17	18.5 ± 0.5	5.5 ± 0.2	3 ± 1.4	3
Spring	1515 ± 10	1611 ± 16	8.2 ± 0.01	1.26 ± 0.1	343 ± 14	15.9 ± 0.4	17.2 ± 0.1	9 ± 5.7	2
Summer	1384 ± 39	1517 ± 50	8.3 ± 0.01	1.85 ± 0.2	304 ± 3	13.6 ± 0.9	28.0 ± 1.2	7 ± 2.6	3
R3W									
Autumn	1686 ± 44	1808 ± 51	8.2 ± 0.01	1.47 ± 0.1	326 ± 19	21.4 ± 1.5	13.5 ± 0.9	6 ±2.8	4
Winter	1672 ± 37	1780 ± 51	8.3 ± 0.03	1.28 ± 0.2	256 ± 20	21.1 ± 1.4	6.0 ± 0.5	3.8 ±1.7	4
Spring	1605 ± 43	1718 ± 51	8.2 ± 0.02	1.44 ± 0.1	381 ± 21	19.3 ± 1.5	18.5 ± 0.4	4.5 ± 2.1	4
Summer	1575 ± 74	1718 ± 81	8.1 ± 0.07	1.92 ± 0.3	444 ± 85	18.6 ± 2.4	28.7 ± 0.3	4.3 ± 0.5	4
R3E									
Autumn	1698 ± 61	1852 ± 58	8.3 ± 0.05	1.79 ± 0.04	289 ± 35	23.0 ± 1.8	14.4 ± 0.2	7 ± 5.7	2
Winter	1801 ± 98	1911 ± 119	8.2 ± 0.03	1.31 ± 0.2	325 ± 28	24.8 ± 3.3	6.6 ± 0.5	3.8 ± 2.8	6
Spring	1742 ± 72	1861 ± 83	8.1 ± 0.02	1.50 ± 0.1	434 ± 23	23.0 ± 2.2	17.6 ± 0.4	6.8 ± 2.6	6
Summer	1623 ± 128	1786 ± 120	8.2 ± 0.1	2.09 ± 0.2	416 ± 103	21.2 ± 3.6	27.3 ± 1.9	3.7 ± 1.8	6

Table 4. Mean values of subsurface CO_2-system parameters in each region. The ± represents the standard deviation of the seasonal average of each parameter in the surface mixed layer in each region. n is the number of stations included when computing the average value in each season.

	DIC^{sub}	TA^{sub}	pH^{sub}	Ω^{sub}	pCO_2^{sub}	S^{sub}	T^{sub}	n
Units	μmol kg^{-1}	μmol kg^{-1}			μatm		°C	
R1								
Autumn	1571 ± 51	1660 ± 52	8.0 ± 0.1	1.16 ± 0.32	389 ± 92	18.7 ± 0.95	14.8 ± 0.5	3
Winter	1682 ± 79	1725 ± 58	7.9 ± 0.1	0.72 ± 0.16	475 ± 163	19.8 ± 1.5	5.4 ± 0.3	3
Spring	1623 ± 193	1583 ± 158	7.5 ± 0.3	0.34 ± 0.19	1602 ± 771	15.6 ± 3.1	13.8 ± 1.1	3
Summer	1674 ± 157	1604 ± 143	7.2 ± 0.2	0.29 ± 0.13	2829 ± 1000	15.3 ± 3.4	23.4 ± 1.4	4
R2								
Autumn	1700 ± 25	1817 ± 23	8.0 ± 0.03	1.42 ± 0.04	366 ± 28	22.1 ± 0.66	14.3 ± 0.2	2
Winter	1661 ± 37	1743 ± 42	8.1 ± 0.1	1.03 ± 0.13	303 ± 40	20.0 ± 1.2	5.49 ± 0.3	3
Spring	1630 ± 93	1688 ± 59	7.9 ± 0.2	0.94 ± 0.30	643 ± 331	18.2 ± 1.6	17.3 ± 0.5	2
Summer	1758 ± 178	1785 ± 151	7.6 ± 0.2	0.80 ± 0.25	1349 ± 480	21.2 ± 3.7	25.3 ± 0.7	3
R3W								
Autumn	1689 ± 61	1811 ± 72	8.1 ± 0.02	1.47 ± 0.12	340 ± 21	21.8 ± 2.0	14.0 ± 0.6	1
Winter	1689 ± 33	1800 ± 45	8.2 ± 0.03	1.3 ± 0.14	256 ± 20	21.7 ± 1.3	5.85 ± 0.2	1
Spring	1647 ± 36	1729 ± 50	7.9 ± 0.1	1.15 ± 0.20	485 ± 69	19.7 ± 1.1	17.7 ± 0.2	2
Summer	1728 ± 174	1800 ± 147	7.7 ± 0.2	1.17 ± 0.26	866 ± 306	21.8 ± 4.4	25.9 ± 2.1	1
R3E								
Autumn	1756 ± 2	1894 ± 14	8.1 ± 0.03	1.63 ± 0.12	347 ± 27	24.3 ± 0.45	14.1 ± 0.1	1
Winter	1865 ± 67	1992 ± 88	8.1 ± 0.1	1.48 ± 0.24	325 ± 39	27.0 ± 2.5	6.79 ± 0.4	3
Spring	1843 ± 92	1955 ± 114	7.9 ± 0.1	1.43 ± 0.25	532 ± 79	25.7 ± 2.9	16.8 ± 1.3	3
Summer	1903 ± 94	2027 ± 112	7.8 ± 0.1	1.61 ± 0.38	690 ± 237	28.0 ± 3.1	21.7 ± 3.7	5

Table 5. Wind speed in each region and season, in m s^{-1}, used to calculate air-sea CO_2 fluxes. Regional surface areas provided in m^2 and determined from Chesapeake Bay Program (2004).

Region	Autumn	Winter	Spring	Summer	Surface Area
R1	5.6	5.5	4.4	5.3	908,849,967
R2	5.6	5.5	4.7	5.1	1,474,652,418
R3W	6.2	4.2	5.8	5.1	949,566,911
R3E	6.2	4.2	5.8	5.1	1,727,035,455

Table 6. Results of the DIC mass balance (μmol kg^{-1} $month^{-1}$) in the mixed layer and whole water column.

	ΔDIC_{total}^{ML}	ΔDIC_{gas}^{ML}	ΔDIC_{circ}^{ML}	ΔDIC_{bio}^{ML}	$\Delta DIC_{total}^{full}$	ΔDIC_{circ}^{full}	ΔDIC_{bio}^{full}
R1							
Autumn - Winter	40	54	-3	-11	77	9	13
Winter - Spring	-150	38	-113	-75	-160	-133	-65
Spring - Summer	81	63	72	-54	106	66	-25
R2							
Autumn - Winter	-16	60	-17	-59	-29	-41	-48
Winter - Spring	-23	15	-26	-12	-54	-85	16
Spring - Summer	-66	29	-37	-58	-2	12	-43
R3W							
Autumn - Winter	-5	38	-4	-39	-5	-6	-37
Winter - Spring	-22	11	-19	-14	-36	-42	-5
Spring - Summer	-14	-13	-9	8	26	27	12
R3E							
Autumn - Winter	35	17	20	-2	70	51	2
Winter - Spring	-20	-11	-20	11	-27	-35	19
Spring - Summer	-58	-3	-31	-24	-28	8	-33

Table 7. Monthly (mol C m^{-2} $month^{-1}$) and annual NCP (mol C m^{-2} $year^{-1}$) in the surface mixed layer and whole water column. The uncertainty associated with NCP in the surface and subsurface waters are 0.08 mol C m^{-2} $month^{-1}$ and 0.07 mol C m^{-2} $month^{-1}$, respectively. Δt between autumn and winter and winter and spring was three months and Δt between spring and summer was two months.

	R1	R2	R3W	R3E	Mainstem
Mixed layer NCP					
Autumn – Winter	0.07	0.35	0.18	0.01	0.15
Winter – Spring	0.47	0.07	0.07	-0.06	0.10
Spring – Summer	0.34	0.34	-0.04	0.13	0.20
Annual	2.3	2.0	0.67	0.11	1.2
Whole water column NCP					
Autumn - Winter	-0.22	-0.06	-0.01	-0.03	-0.07
Winter – Spring	-0.11	-0.06	-0.04	-0.04	-0.06
Spring – Summer	-0.20	-0.09	-0.02	0.05	-0.05
Annual	-1.4	-0.54	-0.19	-0.11	-0.48

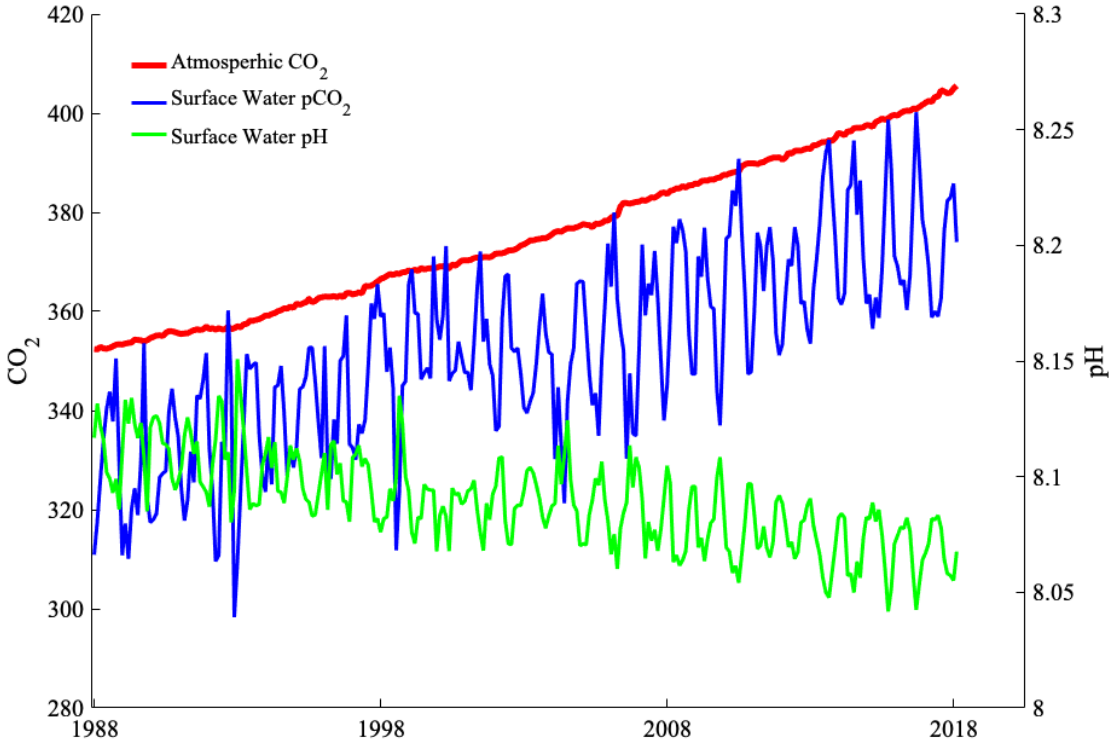

Figure 1. Observed trends in atmospheric CO_2 (red) from the Mauna Loa station on the Big Island of Hawaii and surface water pCO_2 (blue) and pH (green) at the open ocean station Aloha located in the Pacific Ocean, north of the Hawaiian island chain. Surface pCO_2 and pH data used to produce this figure can be found at: http://hahana.soest.hawaii.edu/hot/products/HOT_surface_CO2.txt and concentrations of atmospheric CO_2 can be found at: ftp://aftp.cmdl.noaa.gov/products/trends/co2/co2_mm/mlo.txt.

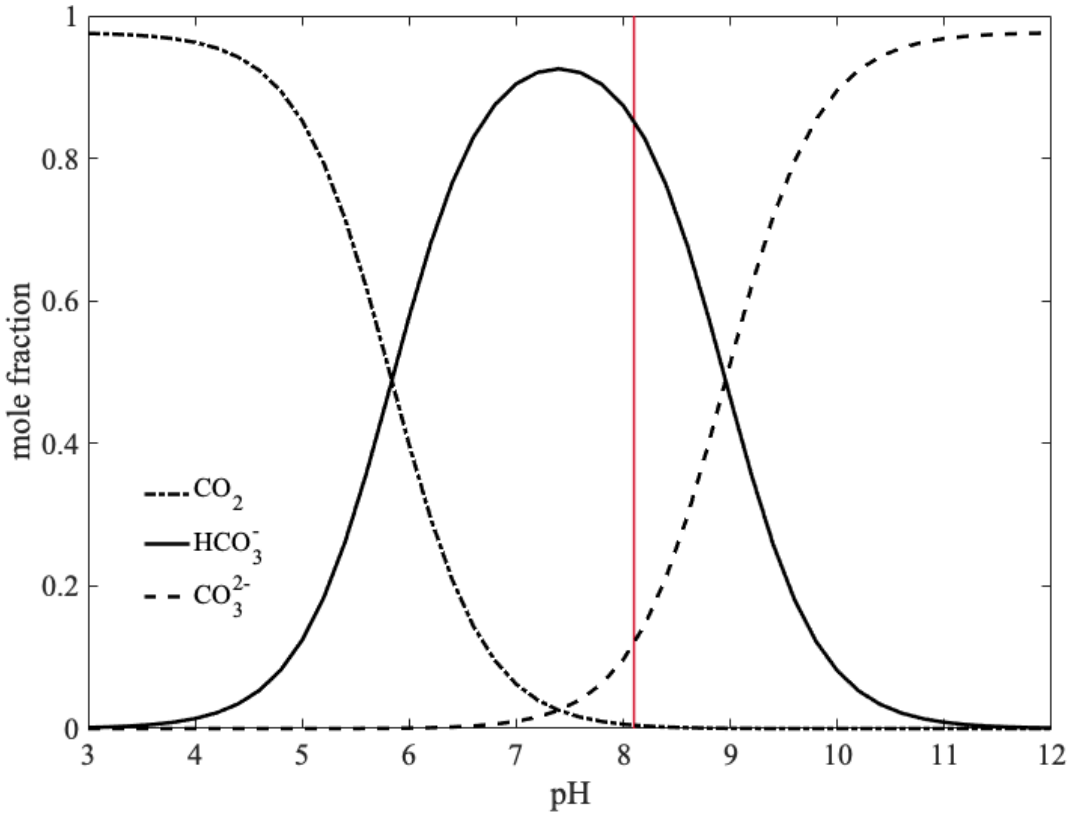

Figure 2. Equilibrium distribution of carbonate species. In current seawater conditions (indicated by the red line), bicarbonate (HCO_3^{-1}) comprises 90% of carbonate species, followed by carbonate (CO_3^{-2}; 9%) and dissolved CO_2 (1%). The relative proportions of each species (H_2CO_3, HCO_3^-, CO_3^{2-}) control pH.

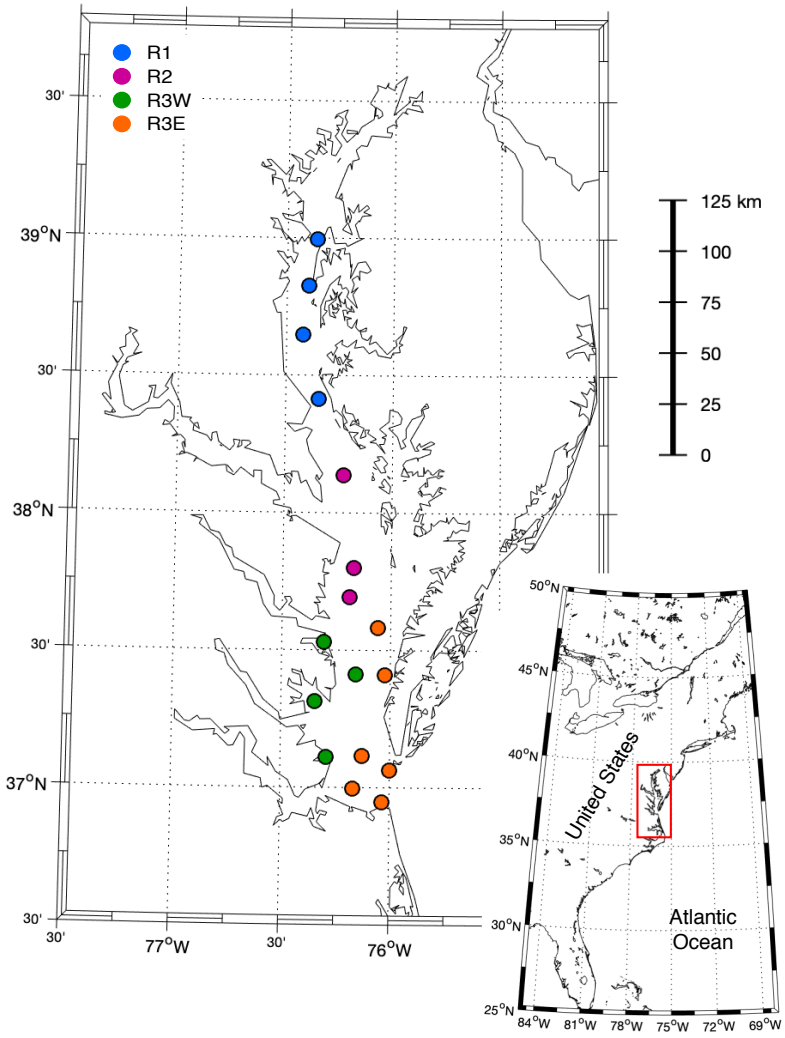

Figure 3. Regional partitioning of the study area: R1 (blue), R2 (magenta), R3E (orange), and R3W (green).

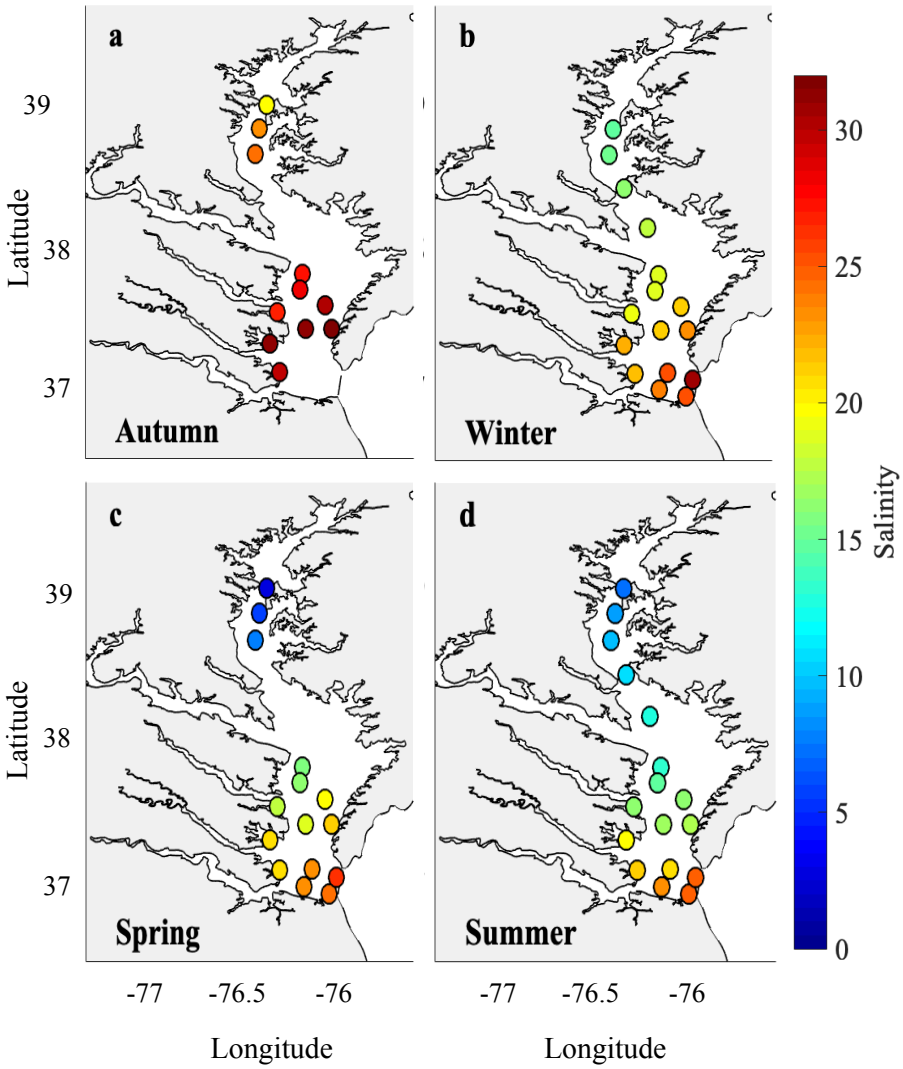

Figure 4. Seasonal surface salinity at each station in the CB mainstem.

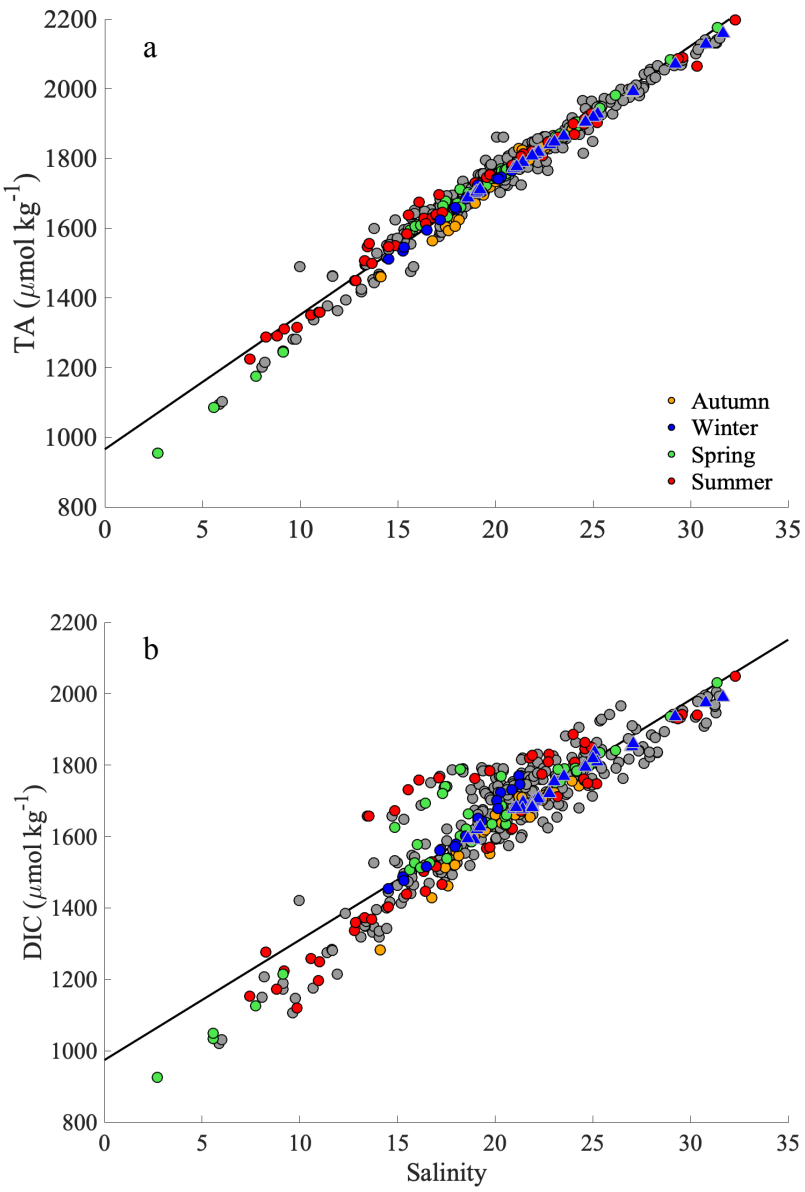

Figure 5. The relationship between TA, DIC, and salinity in the CB mainstem based on all samples collected by VIMS between June 2016 and January 2018 throughout the water column. Seasons used in this analysis are shown by the colored points. Linear regression analysis based on circle symbols yielded the following equation (black line): a) TA = 39(S) + 966 (n= 505, R^2= 0.96, p<0.001, standard error = 7 μmol kg^{-1}); TA_{winter} values computed from this relationship are shown in blue triangles and b) DIC_{sal} = 34(S) + 973 (n= 505, R^2= 0.87, p<0.001, standard error = 12 μmol kg^{-1}). The winter values from VA (i.e., $DIC_{winter} = f(TA_{winter}, pH_{MP})$) are shown in blue triangles.

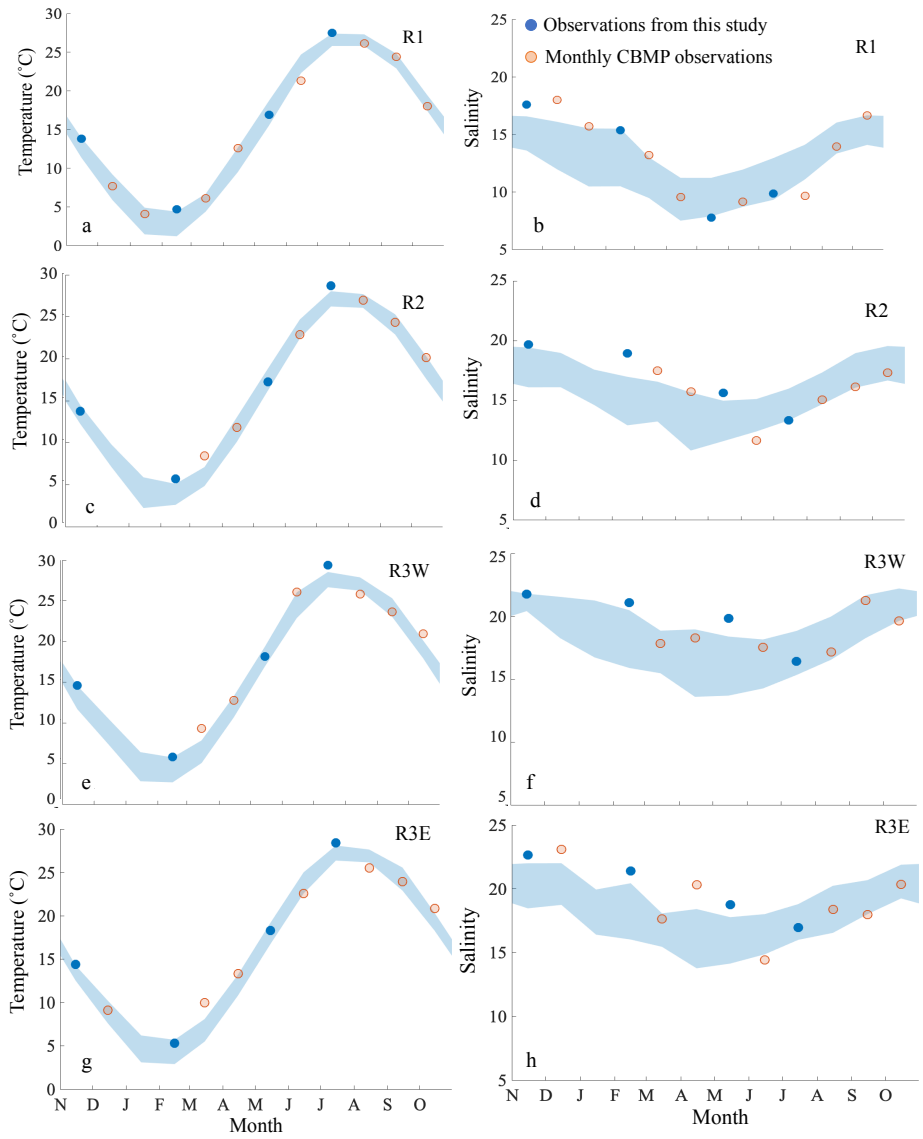

Figure 6. Climatological surface temperature (a, c, e, g) and salinity (b, d, f, h) from CBMP (data from 1984 – 2017), with shaded areas indicating the 25th and 75th percentiles. Seasonal temperature and salinity observations used in this analysis are shown in blue circles; orange circles indicate all other months observed over the study period. Temperature and salinity data from one station per region were used to illustrate the observed seasonality; (a and b) station CB4.2C in R1, (c and d) station CB5.4 in R2, (e and f) station CB6.3 in R3W, and (g and h) station CB7.1S in R3E.

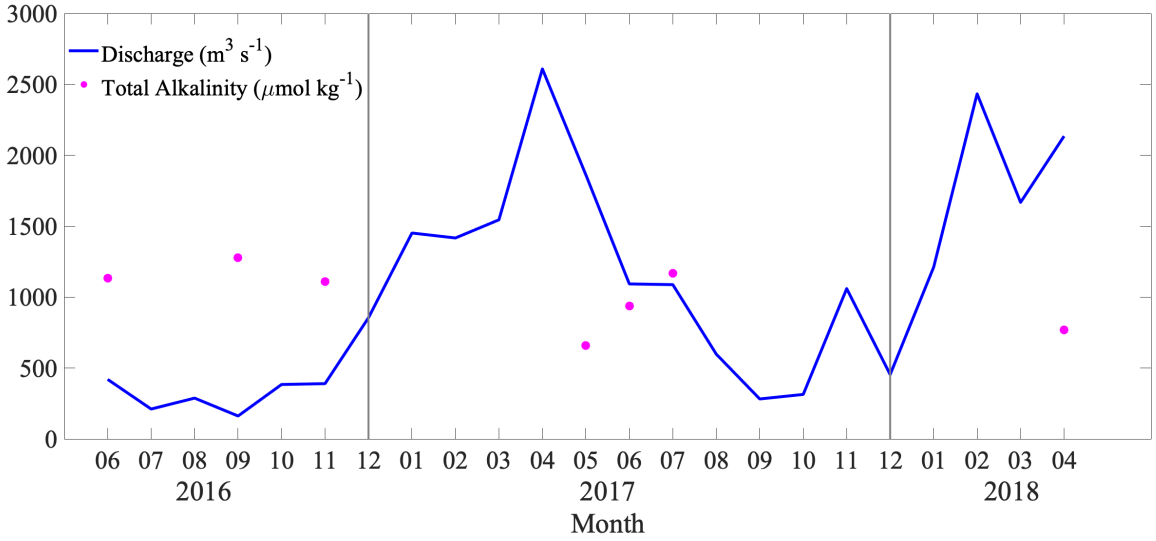

Figure 7. Average monthly discharge (blue) from the Conowingo Dam (USGS station # 01578310) over the duration of discrete TA measurements at station CB1.1 by VIMS (June 2016 – April 2018). Circles indicate when discrete concentrations of surface TA (magenta) was measured at station CB1.1, just south of the Conowingo Dam.

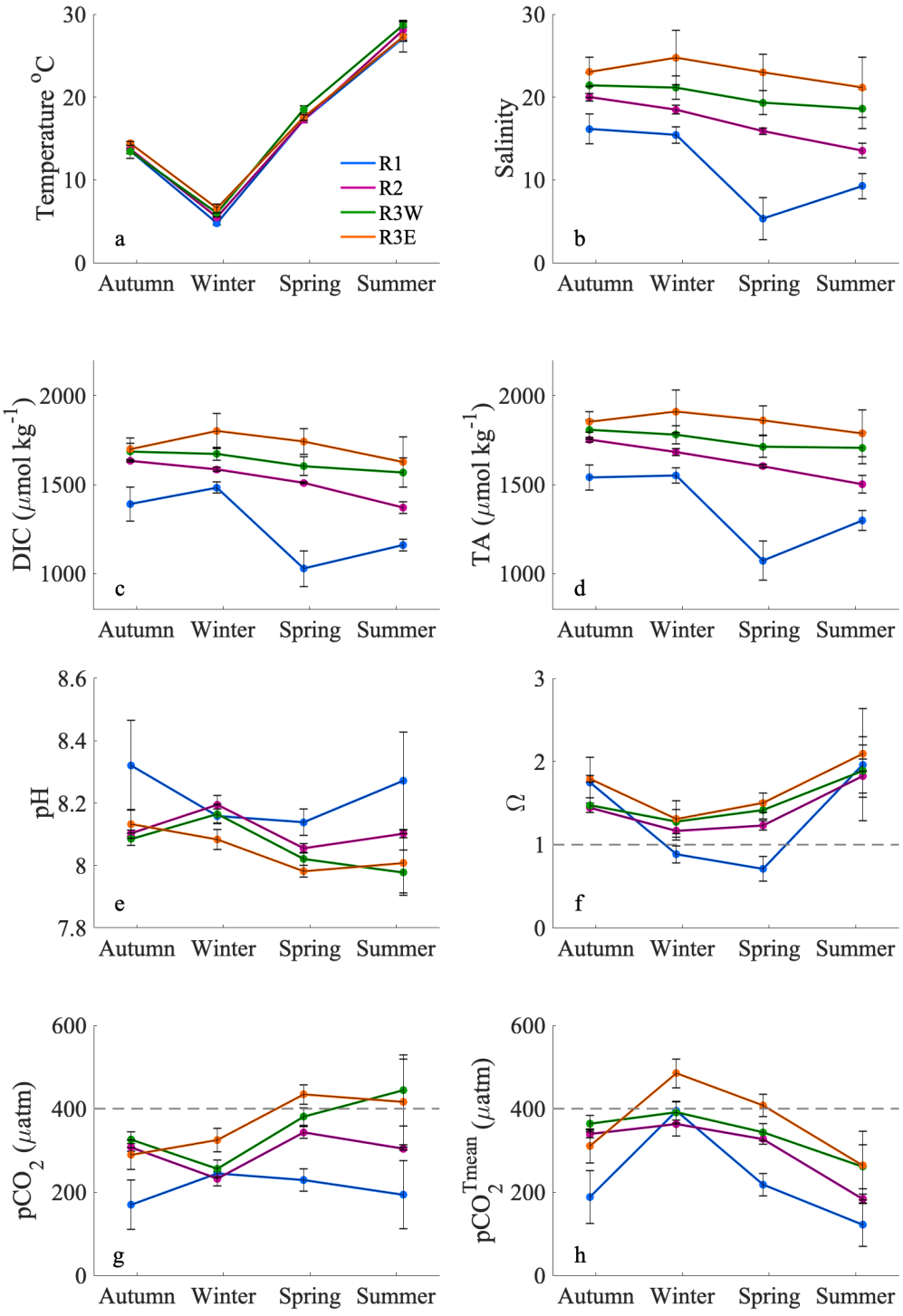

Figure 8. The seasonal cycle in the surface mixed-layer of (a) temperature, (b) salinity, (c) DIC, (d) TA, (e) pH, (f) Ω, (g) pCO_2, and (h) temperature-normalized pCO_2 (pCO_2^{Tmean}) with regions distinguished by color. Values below the dashed line in (f) indicate undersaturation ($\Omega < 1.0$). The dashed lines in (g) and (h) indicate the concentration of atmospheric CO_2 (406 µatm). Error bars represent one standard deviation.

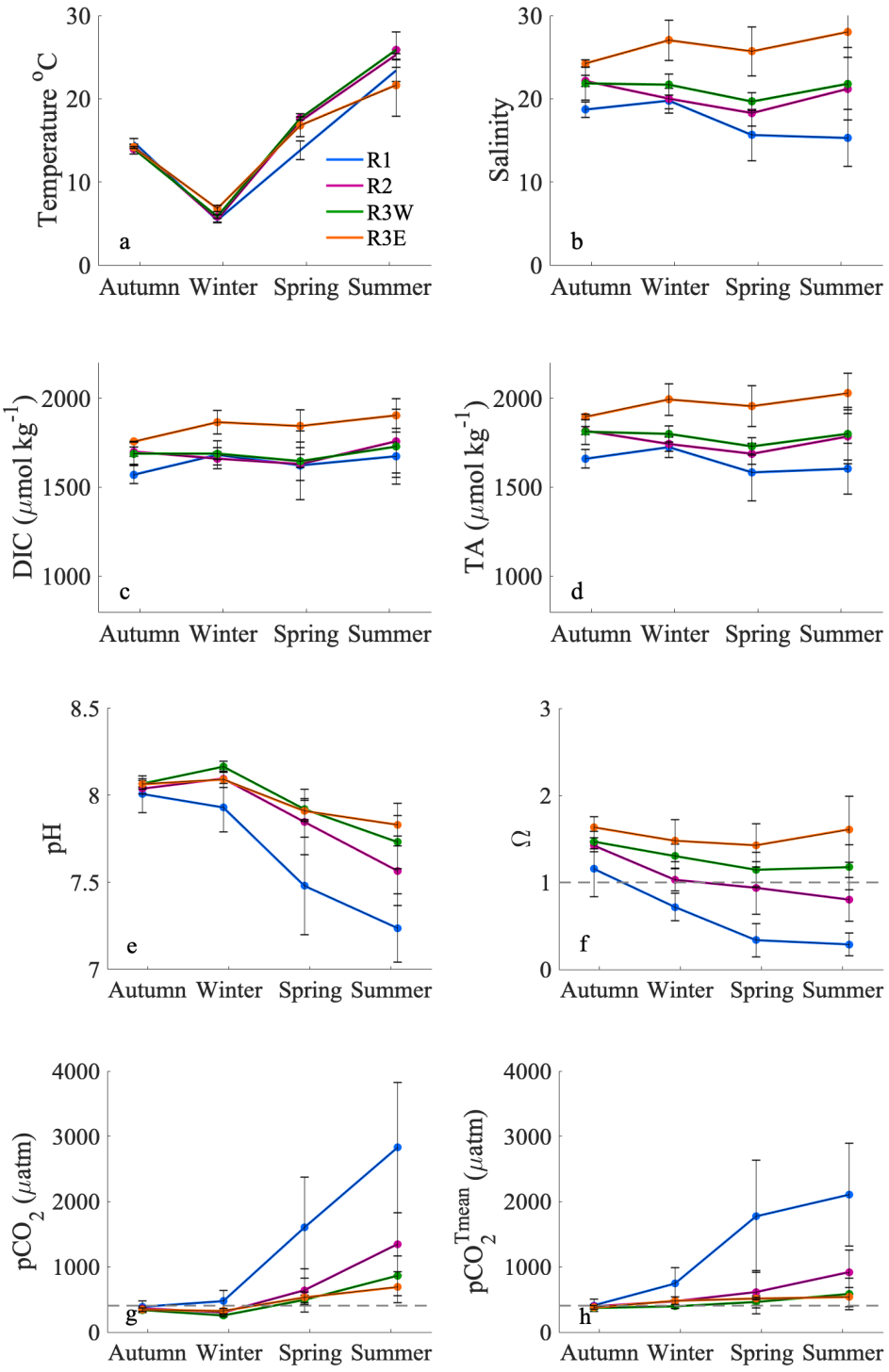

Figure 9. The seasonal cycle throughout the subsurface waters of (a) temperature, (b) salinity, (c) DIC, (d) TA, (e) pH, (f) Ω, (g) pCO_2, and (h) temperature-normalized pCO_2 (pCO_2^{Tmean}) with regions distinguished by color. Values below the dashed line in (f) indicate undersaturation ($\Omega < 1.0$). The dashed lines in (g) and (h) indicate the concentration of atmospheric CO_2 (406 µatm). Error bars represent one standard deviation.

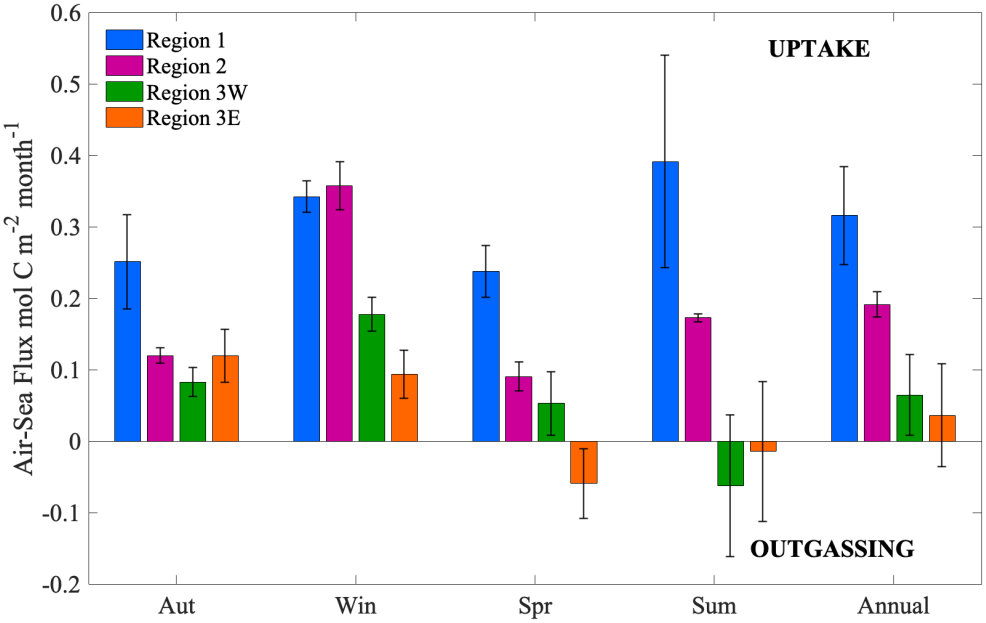

Figure 6. Air-sea CO_2 fluxes throughout the CB mainstem in all season and the annual average. Positive values indicate an uptake of atmospheric CO_2. Error bars represent one standard deviation.

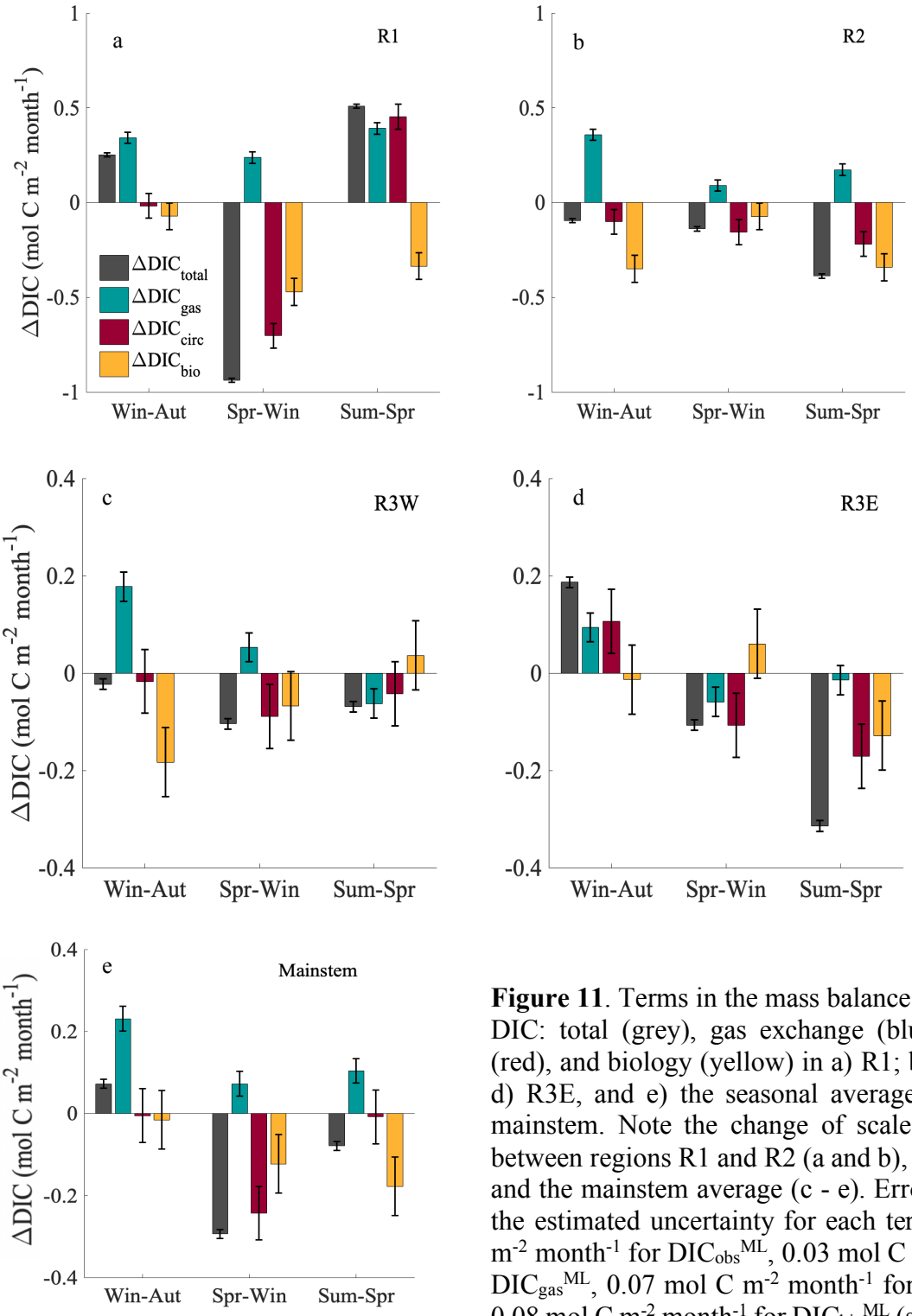

Figure 11. Terms in the mass balance of mixed-layer DIC: total (grey), gas exchange (blue), circulation (red), and biology (yellow) in a) R1; b) R2; c) R3W, d) R3E, and e) the seasonal average for the entire mainstem. Note the change of scale on the y-axes between regions R1 and R2 (a and b), and R3W, R3E and the mainstem average (c - e). Error bars indicate the estimated uncertainty for each term: 0.01 mol C m^{-2} $month^{-1}$ for DIC_{obs}^{ML}, 0.03 mol C m^{-2} $month^{-1}$ for DIC_{gas}^{ML}, 0.07 mol C m^{-2} $month^{-1}$ for DIC_{circ}^{ML}, and 0.08 mol C m^{-2} $month^{-1}$ for DIC_{bio}^{ML} (see section 2.6).

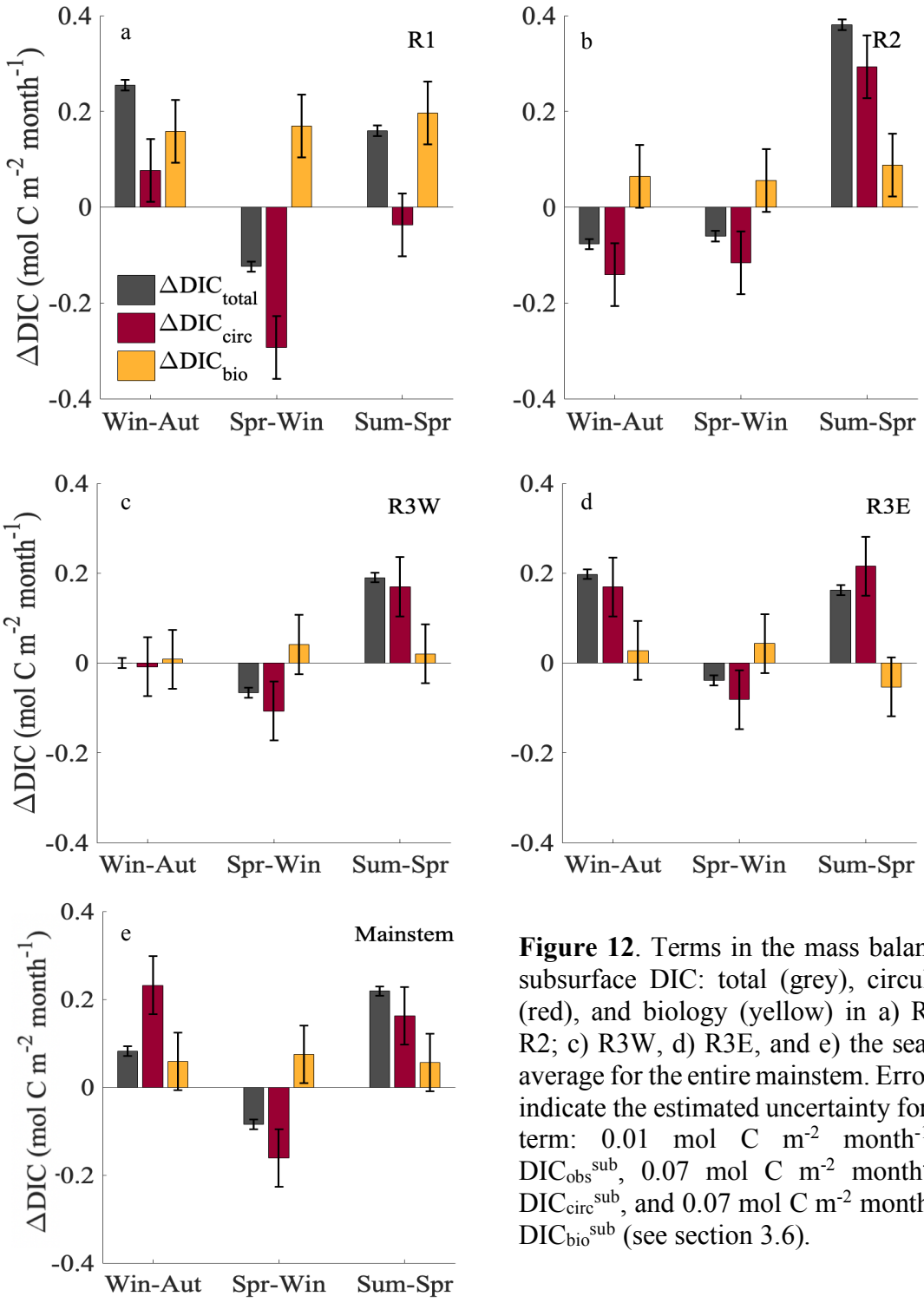

Figure 12. Terms in the mass balance of subsurface DIC: total (grey), circulation (red), and biology (yellow) in a) R1; b) R2; c) R3W, d) R3E, and e) the seasonal average for the entire mainstem. Error bars indicate the estimated uncertainty for each term: 0.01 mol C m^{-2} $month^{-1}$ for DIC_{obs}^{sub}, 0.07 mol C m^{-2} $month^{-1}$ for DIC_{circ}^{sub}, and 0.07 mol C m^{-2} $month^{-1}$ for DIC_{bio}^{sub} (see section 3.6).

Literature Cited:

Bachman, L. J., Lindsey, B., Brakebill, J., & Powars, D. S. (1998). Ground-water Discharge and Base-flow Nitrate Loads of Nontial Streams, and Their Relation to a Hydrogeomorphic Classification of the Chesapeake Bay Watershed, Middle Atlantic Coast. *Water-Resources Investigations Report 98-4059.* United States Department of the Interior, United State Geological Survey.

Borges, A. V. (2005). Do We Have Enough Pieces of the Jigsaw to Integrate CO_2 Fluxes in the Coastal Ocean? *Estuaries*, *28*(1), 3–27. https://doi.org/10.1007/BF02732750

Brodeur, J. R., Chen, B., Su, J., Xu, Y., Hussain, N., Scaboo, K. M., Zhang, Y., Testa, J. M., Cai, W.-J. (2019). Chesapeake Bay Inorganic Carbon: Spatial Distribution and Seasonal Variability. *Frontiers in Marine Science, 6*, 1–17. https://doi.org/10.3389/fmars.2019.00099

Brewer, P. G., & Goldman, J. C. (1976). Alkalinity Changes Generated by Phytoplankton Growth. *Limnology and Oceanography*, *21*(1), 108–117. https://doi.org/10.4319/lo.1976.21.1.0108

Bozec, Y., Thomas, H., Schiettecatte, L.-S., Borges, A., Elkalay, K., & de Baar, H. J. W. (2006). Assessment of the Processes Controlling Seasonal Variations of Dissolved Inorganic Carbon in the North Sea. *Limnology and Oceanography, 51(6),* 2746 - 2762. https://doi/org/10.4319/lo.2006.51.6.2746

Cai, W.-J., Hu, X., Huang, W.-J., Murrell, M. C., Lehrter, J. C., Lohrenz, S. E., Chou, W.-C., Zhai, W., Hollibaugh, J. T., Wang, Y., Pingsan, Z., Xianghui, G., Gunderson, K., Dai, D., & Gong, G.-C. (2011). Acidification of Subsurface Coastal Waters Enhanced by Eutrophication. *Nature Geoscience*, *4*(11), 766–770. https://doi.org/10.1038/ngeo1297

Cai, W.-J., Huang, W.-J., Luther, G. W., Pierrot, D., Li, M., Testa, J., Xue, M., Joesoed, J., Mann, R., Brodeur, J., Xy, Y.-Y., Chen, B., Hussain, N., Waldbrusser, G. G., Cornwell, J., & Kemp, W. M. (2017). Redox Reactions and Weak Buffering Capacity Lead to Acidification in the Chesapeake Bay. *Nature Communications*, *8*(1). 369. https://doi.org/10.1038/s41467-017-00417-7

Cai, W., Dai, M., Wang, Y., Zhai, W., Huang, T., Chen, S., et al. (2004). The biogeochemistry of inorganic carbon and nutrients in the Pearl River estuary and the adjacent northern South China Sea. *Continental Shelf Research*, *24*, 1301–1319. https://doi.org/10.1016/j.csr.2004.04.005

Castro, M. S., Driscoll, C. T., Jordan, T. E., Reay, W. G., & Boynton, W. R. (2003). Sources of Nitrogen to Estuaries in the United States. *Estuaries, 26*(3), 803-814. https://doi.org/10.1007/BF02711991

Chesapeake Bay Program. (2004). *Chesapeake Bay Program Analystical Segmentation Scheme - Revision, Decisions and Rationals 1983 - 2003.*

Chesapeake Bay Program. (2012). *Guide to using Chesapeake Bay program water quality monitoring data*.

Chesapeake Bay Program. (2018). *Tree Cover.* https://www.chesapeakebay.net/state/tree_cover

Da, F., Friedrichs, M. A. M., & St-Laurent, P. (2018). Impacts of Atmospheric Nitrogen Deposition and Coastal Nitrogen Fluxes on Oxygen Concentrations in Chesapeake

Bay. *Journal of Geophysical Research: Oceans*, 123. https://doi.org/10.1029/2018JC014009

Dickson, A. G., & Millero, F. J. (1987). A Comparison of the Equilibrium Constants for the Dissociation of Carbonic Acid in Seawater Media. *Deep Sea Research Part A, Oceanographic Research Papers*, *34*(10), 1733–1743. https://doi.org/10.1016/0198-0149(87)90021-5

Dickson, A. G., Sabine, C. L., & Christian, J. R. (Eds) 2007. *Guide to Best Practices for Ocean CO_2 Measurements*. PICES Special Publication 3, 191 pp.

Doney, S. C. (2010). The Growing Human Footprint on Coastal and Open-Ocean Biogeochemistry. *Science*, *328*(5985), 1512-1516. https://doi.org/10.1126/science.1185198

Dore, J. E., Lukas, R., Sadler, D. W., Church, M. J., & Karl, D. M. (2009). Physical and Biogeochemical Modulation of Ocean Acidification in the Central North Pacific, *106*(30), 12235–12240. https:// doi/10.1073/pnas.0906044106

Feng, Y., Friedrichs, M. A. M., Wilkin, J., Tian, H., Yang, Q., Hofmann, E. E., Wiggert, J. D., & Hood, R. R. (2015). Chesapeake Bay Nitrogen Fluxes Derived From a Land-Estuarine Ocean Biogeochemical Modeling System: Model Description, Evaluation, and Nitrogen Budgets. *Journal of Geophysical Research: Biogeosciences*, 120. https://doi.org/10.1002/2015JG002931

Gobler, C. J., & Baumann, H. (2016). Hypoxia and Acidification in Ocean Ecosystems: Coupled Dynamics and Effects on Marine Life. *Biology Letters*, *12*, 20150976. https://doi.org/10.1098/rsbl.2015.0976

Goodrich, D. M., & Blumberg, A. F. (1991). The Fortnightly Mean Circulation of Chesapeake Bay. *Estuarine, Coastal and Shelf Science*, *32*(5), 451–462. https://doi.org/10.1016/0272-7714/91/050451

Hagy, J. D., Bonton, W. R., Keefe, C. W., & Wood, K. V. (2004). Hypoxia in Chesapeake Bay, 1950 - 2001: Long-term Change in Relation to Nutrient Loading and River Flow. *Estuaries*, *27*(4), 634–658. https://doi.org/10.1007/BF02907650

Harding, L. W., Adolf, J. E., Mallonee, M. E., Miller, W. D., Gallegos, C. L., Perry, E. S., Johnson, J. M., Sellner, K. G., & Paerl, H. W. (2014). Climate Effects on Phytoplankton Floral Composition in Chesapeake Bay. *Estuarine, Coastal and Shelf Science*, *162*, 53–68. https://doi.org/10.1016/j.ecss.2014.12.030

Harding, L. W., Gallegos, C. L., Perry, E. S., Miller, W. D., Adolf, J. E., Mallonee, M. E., & Paerl, H. W. (2016). Long-Term Trends of Nutrients and Phytoplankton in Chesapeake Bay. *Estuaries and Coasts*, *39*(3), 664–681. https://doi.org/10.1007/s12237-015-0023-7

Herrmann, M., Najjar, R. G., Kemp, W. M., Alexander, R. B., Boyer, E. W., Cai, W.-J., et al. (2015). Net ecosystem production and organic carbon balance of U.S. East Coast estuaries: A syntheiss approach. *Global Biogeochemical Cycles, 29,* 96-111. https://doi.org/10.1002/2013GB004736

Hu, X., Li, Q., Huang, W., Chen, B., Cai, W., Rabalais, N. N., & Turner, R. E. (2017). Effects of Eutrophication and Benthic Respiration on Water Column Carbonate Chemistry in a Traditional Hypoxic Zone in the Northern Gulf of Mexico. *Marine Chemistry*, 194. 33-42. https://doi.org/10.1016/j.marchem.2017.04.004

Irby, I. D., Friedrichs, M. A. M., Friedrichs, C. T., Bever, A. J., Hood, R. R., Lanerolle, L. W. J., Ming, L., Linker, L., Scully, M. E., Sellner, K., Shen, J., Testa, J., Wang,

H., Wang, P., & Xia, M. (2016). Challenges Associated with Modeling Low-Oxygen Waters in Chesapeake Bay: A Multiple Model Comparison. *Biogeosciences*, *13*, 2011-2028. https://doi.org/10.5194/bgd-12-20361-2015

Jiang, L.-Q., Cai, W.-J., Feely, R. A., Wang, Y., Guo, X., Gledhill, D. K., Hu, X., Arzayus, F., Chen, F., Hartmann, J., & Zhang, L. (2010). Carbonate Mineral Saturation States Along the U.S. East Coast. *Limnology and Oceanography 55,* 2424-2432. https://doi.org/10.4319/lo.2010.55.6.2424

Joesoef, A., Huang, W. J., Gao, Y., & Cai, W. J. (2015). Air-water Fluxes and Sources of Carbon Dioxide in the Delaware Estuary: Spatial and Seasonal Variability. *Biogeosciences*, *12*(20), 6085–6101. https://doi.org/10.5194/bg-12-6085-2015

Joesoef, A., Kirchman, D. L., Sommerfield, C. K., & Cai, W. (2017). Seasonal Variability of the Inorganic Carbon System in a Large Coastal Plain Estuary. *Biogeosciences*, *14*, 4949–4963. https://doi.org/10.5194/bg-14-4949-2017

Kemp, W. M., Sampou, P. A., Garber, J., Tuttle, J., & Boynton, W. R. (1992). Seasonal Depletion of Oxygen From Bottom Waters of Chesapeake Bay: Roles of Benthic and Planktonic Respiration and Physical Exchange pPocesses. *Marine Ecology Progress Series*, *85*, 137–152. https://doi.org/10.3354/meps085137

Kemp, W. M., Smith, E. M., Marvin-DiPasquale, M., & Boynton, W. R. (1997). Organic Carbon Balance and Net Ecosystem Metabolism in Chesapeake Bay. *Marine Ecology Progress Series*, *150*. 229–248. https://doi.org/10.3354/meps150229

Laruelle, G. G., Dürr, H. H., Slomp, C. P., & Borges, A. V. (2010). Evaluation of Sinks and Sources of CO_2 in the Global Coastal Ocean Using a Spatially-explicit Typology of Estuaries and Continental Shelves. *Geophysical Research Letters*, *37*, L15607. https://doi.org/10.1029/2010GL043691

Laruelle, G. G., Lauerwald, R., Rotschi, J., Raymond, P. A., Hartmann, J., & Regnier, P. (2015). Seasonal Response of Air-Water CO_2 Exchange Along the Land-Ocean Aquatic Continuum of the Northeast North American Coast. *Biogeosciences*, *12*, 1447–1458. https://doi.org/10.5194/bg-12-1447-2015

Laurent, A., Fennel, K., Cai, W.-J., Huang, W.-J., Barbero, L., & Wanninkhof, R. (2017). Eutrophication-induced Acidification of Coastal Waters in the Northern Gulf of Mexico: Insights Into Origin and Processes from a Coupled Physical-biogeochemical Model. *Geophysical Research Letters, 44,* 946 - 956. https://doi.org/10.1002/2016GL071881

Mehrbach, C., Culberson, C., Hawley, J., & Pytkowicz, R. (1973). Measurement of the Apparent Dissociation Constants of Carbonic Acid in Seawater at Atmospheric Pressure. *Limnology and Oceanography*, *18*(6), 897–907. https://doi.org/10.4319/lo.1973.18.6.0897

Najjar, R. G., Herrmann, M., Alexander, R., Boyer, E. W., Burdige, D. J., Butman, D., Cai, W.-J., Canuel, E. A., Chen, R. F., Friedrichs, M. A. M., Feagin, R. A., Griffith, P. C., Hinson, A. L., Holmquist, J. R., Hu, X., Kemp, W. M., Kroeger, K. D., Mannino, A., McCallister, S. L., McGillis, W. R., Mulholland, M. R., Pilskaln, C. H., Salisbury, J., Signorini, S. R., St-Laurent, P., Tian, H., Tzortziou, M., Vlahos, P., Wang, Z. A., & Zimmerman, R. C. (2018). Carbon Budget of Tidal Wetlands, Estuaries, and Shelf Waters of Eastern North America. *Global Biogeochemical Cycles*, 32. https://doi.org/10.1002/2017GB005790

Najjar, R. G., Pyke, C. R., Adams, M. B., Breitburg, D., Hershner, C., Kemp, M.,

Howarth, R., Mulholland, M. R., Paolisso, M., Secor, D., Sellner, K., Wardrop, D., & Wood, R. (2010). Potential Climate-change Impacts on the Chesapeake Bay. *Estuarine, Coastal and Shelf Science*, *86*, 1–20. https://doi.org/10.1016/j.ecss.2009.09.026

Nightingale, P. D., Malin, G., Law, C. S., Watson, A. J., Liss, P. S., Liddicoat, M. I., Boutin, J., & Upstill-Goddard, R. C. (2000). In Situ Evaluation of Air-Sea Gas Exchange Parameterizations Using Novel Conservative and Volatile Tracers. *Global Biogeochemical Cycles*, *14*, 373–387. https://doi.org/10.1029/1999GB900091

Orr, J. C., Fabry, V. J., Aumont, O., Bopp, L., Doney, S. C., Feely, R. A., Gnanadesikan, A., Gruber, N., Ishida, A., Joos, F., Key, R. M., Lindsay, K., Maier-Reimer, E., Matear, R., Monfray, P., Mouchet, A., Najjar, R. G., Plattner, G.-K., Rodgers, K. B., Sabine, C. L., Sarimentio, J. L., Schlitzer, R., Slater, R. D., Totterdel, I. J., Weirig, M.-F., Yamanaka, Y., & Yool, A. (2005). Anthropogenic ocean acidification over the twenty-first century and its impact on calcifying organisms. *Nature*, *437*, 681–686. https://doi.org/10.1038/nature04095

Raymond, P. A., Bauer, J. E., & Cole, J. J. (2000). Atmospheric CO_2 Evasion, Dissolved Inorganic Carbon Production, and Net Heterotrophy in the York River Estuary. *Limnology and Oceanography*, *45*(8), 1707–1717. https://doi.org/10.4319/lo.2000.45.8.1707

Reay, W. G. (2009). Water Quality within the York River Estuary. *Journal of Coastal Research*, *10057*, 23–39. https://doi.org/10.2112/1551-5036-57.sp1.23

Schneider, B. (2011). The CO_2 System of the Baltic Sea: Biogeochemical Control and Impact of Anthropogenic CO_2, *Global Change and Baltic Coastal Zones, Chapter 3*. 33–49. https://doi.org/10.1007/978-94-007-0400-8_3

Schultz, G. E. (1999). Bacterial dynamics and community structure in the York River estuary. *Dissertations, Theses, and Masters Projects*. Paper 1539616843. https://doi.org/10.25773/v5-e0ce-tt62

Shadwick, E. H., Friedrichs, M. A. M., Najjar, R. G., De Meo, O. A., Friedman, J. R., Da, F., & Reay, W. G. (2019). High Frequency CO_2-System Variability in the Chesapeake Bay: Winter-to-Spring Transition at the York River Spit. *In revision.*

Shadwick, E. H., Thomas, H., Azetsu-Scott, K., Greenan, B. J., Head, E., & Horner, E. (2011). Seasonal Variability of Dissolved Inorganic Carbon and Surface Water *p*CO2 in the Scotian Shelf Region of the Northwestern Atlatnic. *Marine Chemistry, 124,* 23-37. https://doi.org/10.1016/j.marchem.2010.11.004

Sharp, J. H., Culberson, C. H., & Church, T. M. (1982). The Chemistry of the Delaware Estuary, General Considerations. *Limnology and Oceanography*, *27*(6), 1015–1028. https://doi.org/10.4319/lo.1982.27.6.1015

Shen, C., Testa, J. M., Li, M., Cai, W.-J., Waldbusser, G. G., Ni, W., Kemp, W. M., Cornwell, J., Chen, B., Brodeur, J., & Su, J. (2019). Controls on Carbonate System Dynamics in a Coastal Plain Estuary: A Modeling Study. *Journal of Geophysical Research: Biogeosciences*, *124*, 61–78. https://doi.org/10.1029/2018JG004802

Sin, Y., Wetzel, R. L., & Anderson, I. C. (1999). Spatial and Temporal Characteristics of Nutrient and Phytoplankton Dynamics in the York River Estuary, Virginia: Analyses of Long-term Data. *Estuaries*, *22*, 260–275. https://doi.org/10.2307/1352982

Sunda, W. G., & Cai, W.- J. (2012). Eutrophication Induced CO_2-Acidification of

Subsurface Coastal Waters: Interactive Effects of Temperature, Salinity, and Atmospheric pCO_2. *Environmental Science and Technology*, *46*, 10651–10659. https://doi.org/10.1021/es300626f

Takahashi, T., Sutherland, S. C., Sweeney, C., Poisson, A., Metzl, N., Tilbrook, B., Bates, N., Wanninkhof, R., Feely, R. A., Sabine, C. L., Olafsson, J., & Nojiri, Y. (2002). Global Sea-Air CO_2 Flux Based on Climatological Surface Ocean pCO_2, and Seasonal Biological and Temperature Effects. *Deep-Sea Research Part II: Topical Studies in Oceanography*, *49*, 1601–1622. https://doi.org/10.1016/S0967-0645(02)00003-6

Thomas, H., Bozec, Y., Elkalay, K., & De Baar, H. J. W. (2004). Enhanced Open Ocean Storage of CO_2 from Shelf Sea Pumping. *Science*, *304*, 1005–1008. https://doi.org/10.1126/science.1095491

Thomas, H., Bozec, Y., Elkalay, K., Baar, H. J. W. De, Borges, A. V, & Schiettecatte, L. (2005). Controls of the Surface Water Partial Pressure of CO_2 in the North Sea. *Biogeosciences*, *2*, 323–334. https://doi.org/10.5194/bg-2-323-2005

United States Department of Agriculture (2018). *Chesapeake Bay Watershed Action Plan.*

United States Geological Survey (2018). *Freshwater Flow into the Chesapeake Bay.* https://www.usgs.gov/centers/cba/science/freshwater-flow-chesapeake-bay?qt-science_center_objects=1#qt-science_center_objects

van Heuven, S., Pierrot, D., Rae, J. W. B., Lewis, E., & Wallace, D. W. (2011). *Matlab program developed for CO2 system calculations* (Tech. Rep.). ORNL/CDIAC.

Wanninkhof, R. (2014). Relationship Between Wind Speed and Gas Exchange Over the Ocean Revisited. *Limnology and Oceanography: Methods*, *12*, 351–362. https://doi.org/10.4319/lom.2014.12.351

Wanninkhof, R., & McGillis, W. R. (1999). A Cubic Relationship Between Air-Sea CO_2 Exchange and Wind Speed. *Geophysical Research Letters*, *26*, 1889–1892. https://doi.org/10.1029/1999GL900363

Weiss, R. F. (1974). Carbon Dioxide in Water and Seawater: The Solubility of a Non-ideal Gas. *Marine Chemistry*, *2*, 203–215. https://doi.org/10.4319/lo.1999.44.4.1148

Xu, J., Long, W., Wiggert, J. D., Lanerolle, L. W. J., Brown, C. W., Murtugudde, R., & Hood, R. R. (2012). Climate Forcing and Salinity Variability in Chesapeake Bay, USA. *Estuaries and Coasts*, *35*, 237–261. https://doi.org/10.1007/s12237-011-9423-5

Xu, Y., Cai, W., Gao, Y., Wanninkhof, R., Salisbury, J., Chen, B., Reimer, J. J., Gonski, S., & Hussain, N. (2017). Short-term Variability of Aragonite Saturation State in the Central Mid-Atlantic Bight. *Journal of Geophysical Research:Oceans*, 4274–4290. https://doi.org/10.1002/2013JC009262.Received

Zeebe, R., & Wolf-Galdrow, D. (2001). *CO_2 in Seawater: Equilbrium, Kinetics, Isotopes*. *Elsevier Oceanography Series* (Vol. 65).

Zimmerman, A. R., & Canuel, E. A. (2000). A Geochemical Record of Eutrophication and Anoxia in Chesapeake Bay Sediments: Anthropogenic Influence on Organic Matter Composition. *Marine Chemistry*, *69*, 117–137. https://doi.org/10.1016/S0304-4203(99)00100-0